Geophysical Journal International

Geophys. J. Int. (2014) **199,** 178–199
GJI Geodynamics and tectonics

doi: 10.1093/gji/ggu251

Electrical resistivity structure of the Great Slave Lake shear zone, northwest Canada: implications for tectonic history

Yaotian Yin,[1] Martyn Unsworth,[2] Mitch Liddell,[2] Dinu Pana[3] and James A. Craven[4]

[1]*China University of Geosciences, Beijing, Peoples Republic of China*
[2]*Department of Physics, University of Alberta, Edmonton, Canada. E-mail: unsworth@ualberta.ca*
[3]*Alberta Geological Survey, Alberta Energy Regulator, AB T6E 2E1, Canada*
[4]*Natural Resources Canada, 615 Booth Street, Ottawa, ON K1A0E9, Canada*

Accepted 2014 June 27. Received 2014 June 26; in original form 2014 February 18

SUMMARY

Three magnetotelluric (MT) profiles in northwestern Canada cross the central and western segments of Great Slave Lake shear zone (GSLsz), a continental scale strike-slip structure active during the Slave-Rae collision in the Proterozoic. Dimensionality analysis indicates that (i) the resistivity structure is approximately 2-D with a geoelectric strike direction close to the dominant geological strike of N45°E and that (ii) electrical anisotropy may be present in the crust beneath the two southernmost profiles. Isotropic and anisotropic 2-D inversion and isotropic 3-D inversions show different resistivity structures on different segments of the shear zone. The GSLsz is imaged as a high resistivity zone (>5000 Ω m) that is at least 20 km wide and extends to a depth of at least 50 km on the northern profile. On the southern two profiles, the resistive zone is confined to the upper crust and pierces an east-dipping crustal conductor. Inversions show that this dipping conductor may be anisotropic, likely caused by conductive materials filling a network of fractures with a preferred spatial orientation. These conductive regions would have been disrupted by strike-slip, ductile deformation on the GSLsz that formed granulite to greenschist facies mylonite belts. The pre-dominantly granulite facies mylonites are resistive and explain why the GSLsz appears as a resistive structure piercing the east-dipping anisotropic layer. The absence of a dipping anisotropic/conductive layer on the northern MT profile, located on the central segment of the GSLsz, is consistent with the lack of subduction at this location as predicted by geological and tectonic models.

Key words: Electrical properties; Magnetotellurics; Transform faults; North America.

1 INTRODUCTION

Large-scale strike-slips faults/shear zones are a major component of continental plate tectonics. They can be lithospheric in scale and accommodate horizontal displacements of hundreds to thousands of kilometres. Examples include the San Andreas Fault in California, the Tintina-Northern Rocky Mountain trench in the Canadian Cordillera, the North Anatolian Fault in Turkey, the Altyn Tagh Fault in China and the Dead Sea Transform in Jordan (Armijo *et al.* 1999; Unsworth *et al.* 1999; Bedrosian *et al.* 2001; Ritter *et al.* 2003a; Gabrielse *et al.* 2006). Geological studies of modern transform faults are hindered by the limited access to the unexposed structural levels of the faults. Drilling programs such as SAFOD (Hickman *et al.* 2004) have sought to address this problem, but to date drilling has only reached the shallow parts of the fault zone. Over the last few decades, a number of studies have shown that exhumed crustal-scale shear zones in Precambrian terranes are good analogues for the deeper levels of modern continental-scale faults (Sibson 1977, 1983). Fig. 1 shows the model of Sibson (1977) with a narrow zone of brittle deformation in the upper crust and a wider zone of ductile deformation at greater depths.

Geophysical studies of modern shear zones using a range of techniques have revealed information that complements geological and drilling studies. For example, seismic reflection has been used to locate and define the geometry of faults (e.g. Williams *et al.* 2003; Harris 2009). However, zones of fractured rock can often make interpretation very difficult (McBride & Brown 1986). Electromagnetic methods are useful for imaging fault zones because they are sensitive to the presence of fluids. The magnetotelluric (MT) method is the only electromagnetic exploration technique that can be used to study electrical resistivity structure at depths greater than a few kilometres, and has been used to investigate the internal structure of active fault zones (e.g. Unsworth & Bedrosian 2004a). A fault-zone conductor (FZC) is often, but not always, observed in the upper crustal part of strike-slip faults (Unsworth & Bedrosian 2004b). This is believed to be associated with the elevated porosity of the damaged zone which becomes saturated with fluids. Examples include the San Andreas Fault (Mackie *et al.* 1994; Unsworth *et al.* 1999, 2000; Bedrosian *et al.* 2004) and the West Fault in

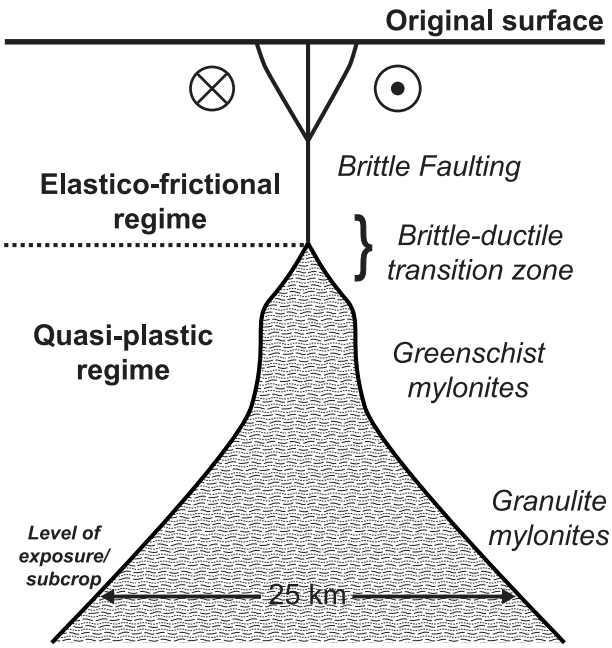

Figure 1. Schematic model of a vertical profile through an idealized crustal-scale transcurrent shear zone (after Sibson 1977).

Northern Chile (Janssen *et al.* 2002; Hoffman-Rothe *et al.* 2004). The active Dead Sea Transform in Jordan demonstrates an impermeable seal to cross-fault fluid transport rather than a FZC (Ritter *et al.* 2003b; Meqbel *et al.* 2013). Conductors are also observed in fault zones in the middle and lower crust and have been interpreted as fluid migration pathways (Becken *et al.* 2008) or zones of active shearing (Bai *et al.* 2010).

In relating the geological study of ancient faults and the geophysical studies of modern faults, problems can arise from compositional/mineralogical changes that may have occurred since the fault zone became inactive. This issue can be addressed by using geophysical methods to study inactive shear zones—allowing a more objective comparison of mapped geological features and geophysical data. Exhumed fossil shear zones can reveal the anatomy of the mid- or lower-crustal shear zones and the composition of the adjacent crust at the time when they were active (Rutter *et al.* 1995). Low-resistivity zones are often imaged in the lower crust and have been suggested to be caused by interconnected graphite films (Yardley & Valley 1997) or aqueous saline fluids (Jones 1992; Wannamaker 2000) that were connected by shearing. In addition, lower-crustal electrical anisotropy may result from preferred orientations of fluidized material or graphitized shear zones. The fossil Waterberg Fault/Omaruru Lineament in Namibia was imaged as a subvertical, 14-km-deep, 10-km-wide zone of high and anisotropic conductivity, which was explained by the presence of graphite along former shear planes (Weckmann *et al.* 2003). The Great Glen Fault formed at the end of the Silurian by the collision of Laurentia and Baltica, and is characterized by a major crustal conductor (Kirkwood *et al.* 1981). In summary, low electrical resistivity, sometimes associated with anisotropy, is regularly observed within exhumed fault/shear zones.

The Great Slave Lake shear zone (GSLsz) in northwest Canada is a continental scale fossil shear zone, 1300 km long by up to 25 km wide and located on the western Canadian Shield (Gibb 1978; Hanmer 1988; Fig. 2). The petrological and structural features of its exposed segment are well understood, making the GSLsz a natural laboratory for geophysical investigations of the lithospheric structure of a continental transform fault. In this paper, we present 2-D and 3-D resistivity models derived from MT data for the lithospheric structure of the GSLsz and discuss them in the context of geological studies of this shear zone.

2 GEOLOGICAL AND TECTONIC SETTING

The GSLsz can be traced in outcrop for over 200 km along strike (Reinhardt 1969; Hanmer & Lucas 1985; Hanmer & Connelly 1986; Hanmer 1988; Hanmer & Needham 1988; Hanmer *et al.* 1992). Its magnetic and gravimetric signature continues to the southwest under the sedimentary cover of the Western Canada sedimentary basin (WCSB), to the foothills of the Canadian Cordillera (Geological Survey of Canada 1981, 1984, 1987; Hoffman 1988, 1989). The GSLsz marks the boundary between the southeastern margin of the Archean Slave Craton and the western edge of the Archean Rae Craton (Hoffman 1987, 1988; Fig. 2a). These cratons are interpreted as Archean continental fragments that were sutured together between 2.0 and 1.8 Ga during the assembly of Laurentia (Hoffman 1988, 1989). In the plate tectonics scenario proposed for the region shown in Fig. 3, eastward subduction of the intervening oceanic crust led to the development of the *ca*. 2.5–2.3 Ga Arrowsmith and the 1.99–1.92 Ga Thelon/Taltson magmatic arcs on the western margin of the Rae continent (Hoffman 1988, 1989; Ross 2002; Berman *et al.* 2013). By analogy with the India-Asia collision, the Slave continent was interpreted to have acted as a rigid indentor that deformed the rigid-plastic Rae continent, with dextral strike-slip along the GSLsz accommodating displacement at the southern boundary of the indentor (Gibb 1978). The GSLsz was initiated as a transcurrent fault and later acted as a transform fault within the Thelon-Taltson magmatic arc at the leading edge of the Rae continent during 2.02–1.91 Ga oblique convergence and collision with, and indentation by, the Slave continent (Hoffman *et al.* 1986; Hoffman 1987, 1988; van Breemen *et al.* 1987). Subsequent convergence on the western side of the Slave craton formed the Great Bear magmatic arc and the Wopmay orogen (1.92 Ga–1.84 Ga; Hoffman 1980). Alternative regional tectonic models highlight the lack of evidence for subduction between the Archean Slave and Rae domains and imply that the GSLsz was an intracontinental crustal-scale transcurrent shear zone (Chacko *et al.* 2000; De *et al.* 2000; Pană *et al.* 2007).

Early phases of deformation (1.98–1.92 Ga) resulted in 700 km of ductile strike-slip deformation, whereas subsequent brittle deformation along the colocated Hay River-MacDonald fault system accommodated an additional 75–125 km of dextral offset (Hoffman 1987; Hanmer *et al.* 1992, Fig. 3c). Most of the major strike-slip fault systems in Western Canada experienced minor reactivation during the Laramide Orogeny (Peirce *et al.* 2001). The reactivation of the GSLsz as the Hay River fault zone was described by Muir & Davis (1992).

Southeast of the GSLsz, regional magnetic data and sparse basement core geochronological data have been interpreted by Ross *et al.* (1991, 1994, 2000) as defining a record of terrane accretion. Their model proposed that in this region the Taltson magmatic zone was formed by the convergence of the composite, largely magmatic Buffalo Head terrane (BHT) with the Rae continent. The BHT comprises *ca*. 2.32–2.0 Ga metaplutonic and subordinate felsic metavolcanic rocks and is characterized by sinuous aeromagnetic patterns and discrete subdomains, suggesting that it is a complex

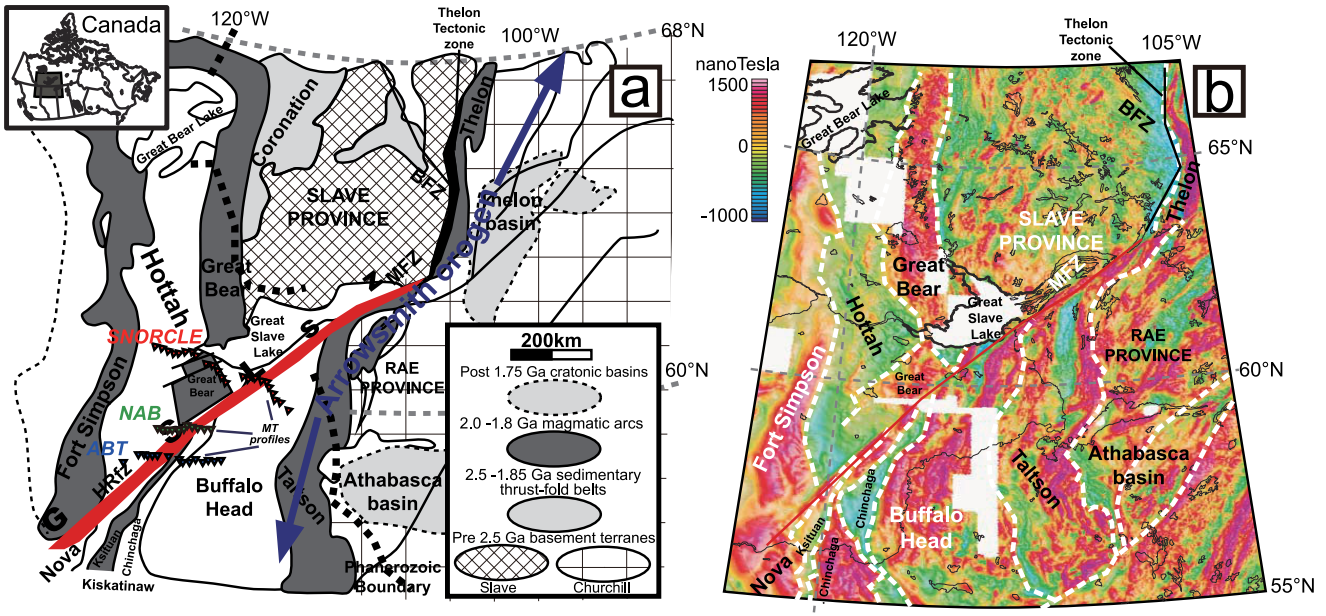

Figure 2. (a) Major subdivisions and tectonic framework of northwest Canadian Shield, after Hanmer (1988). MT site locations of the three profiles used in this study are shown by black triangles. (b) Aeromagnetic anomaly map of northwest Canadian Shield, after Eaton & Hope (2003).

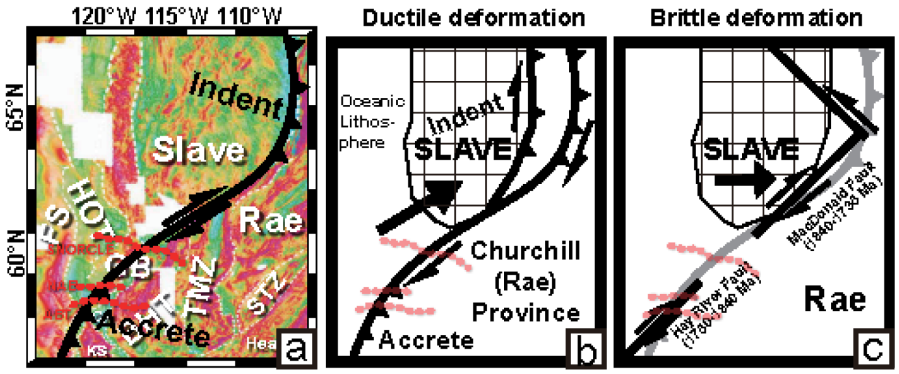

Figure 3. Cartoon of the geodynamic evolution of the GSLsz (modified from Ross & Eaton 2001). Aeromagnetic data from Geiger & Cook (2001).

region of crustal fragments. West of the BHT, the Chinchaga Low is composed of 2.18–2.09 Ga metaplutonic and metasedimentary gneiss with a uniform negative aeromagnetic signature. Sharp aeromagnetic boundaries on either sides of the Chinchaga Low suggest faulted contacts. The Ksituan High, to the west of the Chinchaga Low, has a strong, positive aeromagnetic expression that is typical of calc-alkaline magmatic belts. Plutonic rocks that are characteristic of this domain have ages between 1.98 and 1.90 Ga. The belt can be traced to the northeast, where it is eventually truncated by the GSLsz (Hay River fault; Fig. 2). Two sliver-shaped aeromagnetic anomalies, one negative (Kiskatinaw Low) and the other positive (Nova Domain), are wedged between the GSLsz and the Ksituan High. The buried, and poorly defined, Hay River terrane was suggested to be made of granitic material corresponding to a magnetic low inferred from drill-core and potential field data (Ross *et al.* 2000).

3 GEOLOGICAL STRUCTURE OF THE GSLsz

The exposed segment of the GSLsz has been geologically mapped in detail for over 200 km along strike (Reinhardt 1969; Hanmer & Lucas 1985; Hanmer & Connelly 1986; Hanmer & Needham 1988; Hanmer 1988; Hanmer *et al.* 1992). It has been recognized as a 25-km-wide NE trending corridor of granulite to lower greenschist facies, mylonitic rocks. The protolith of the GSLsz mylonites consists mainly of granite, granodiorite and subordinate paragneiss. The wall rocks on either side of the GSLsz are quite different. On the northwest side the wall rock consists of predominantly Archean leucogranites (2.55 Ga), with rafts of supracrustal rocks (Hanmer *et al.* 1992). On the southeast side of GSLsz, the wall rock consists of mylonitized Early Proterozoic granites (1.96 Ga) of the Taltson magmatic zone, including the Snowdrift granite. All components of the wall rock are cut by a swarm of upright, mafic dykes, oriented parallel to GSLsz; the dykes are closely spaced near the shear zone and more widely spaced further away throughout the East Arm of Great Slave Lake, where their age is constrained to be younger than 2.2–2.1 Ga (Hoffman *et al.* 1977, Bowring *et al.* 1984). Sets of dykes can result in electrically anisotropic structures, since they can be composed of alternating planes of different conductivity parallel to the strike direction (Wannamaker 2005).

The shear zone is characterized by (i) a 25-km-wide belt of annealed ductile mylonites with anhydrous granulite paragenesis and amphibolite facies paragenesis, and (b) narrower bands,

1–1.5 km wide of retrogressive, hydrated greenschist facies mylonite. The association of fault rocks formed at different structural levels in the crust (granulite, amphibolite, greenschist facies mylonites and breccia/cataclasite) within this wide zone of strain concentration indicates progressive syntectonic exhumation during protracted strike-slip displacement (Hanmer 1988). Fig. 2 shows that there is significant along strike structural and petrological complexity. The model of Sibson (1977) shown in Fig. 1 predicts that the width of a shear zone broadens with depth as temperature increases. The model implies that during the late development of presently exposed greenschist mylonite belts and brittle faults in the upper crust, wide belts of granulite mylonite were being formed in the lower crust.

The trace of the GSLsz in the study area beneath the WCSB is inferred from potential field data (Hoffman 1988, 1989). A greenschist facies mylonite recovered from a drillhole along this lineament yielded an $^{40}Ar/^{39}Ar$ muscovite age of *ca*. 1722 Ma and confirmed the continuation of the GSLsz beneath the Phanerozoic cover of the WCSB (Plint & Ross 1993). It is anticipated that bands of granulite to greenschist facies mylonite, similar to those on the exposed segment, characterize the GSLsz segment buried under the WCSB, but this extrapolation must be used with caution. As previous studies of major strike-slip fault systems have shown, these rocks may exhibit differences in electrical resistivity and make electromagnetic methods a useful tool for understanding the subsurface structure of the GSLsz (Ritter *et al.* 2004).

4 PREVIOUS GEOPHYSICAL STUDIES OF GSLsz AND SURROUNDING REGIONS

The current understanding of the structure and geological history of the crust in the study area is based on regional LITHOPROBE geophysical transects, such as Slave-Northern Cordillera Lithospheric Evolution (SNORCLE) and Alberta Basement Transect (ABT), integrated with geological and geochronological studies (e.g. Ross *et al.* 1991; Pilkington *et al.* 2000). Potential field studies define the location and orientation of the GSLsz on the continental scale, including covered areas and depict the heterogeneity of the shear zone along its strike and dip (Hoffman 1988; Geiger & Cook 2001). For example, between the northwestern MacDonald and the southeastern Hay River fault zones, the GSLsz exhibits significant aeromagnetic variability along strike (Fig. 3 and also fig. 3 of Eaton & Hope 2003). In northwest Alberta, the GSLsz is defined as a positive magnetic anomaly (Geiger & Cook 2001), whereas to the northeast along the shore of Great Slave Lake it is characterized as a negative magnetic anomaly. Basement drill core samples correlated with magnetic anomalies shows that the polarity of the magnetic anomaly can depend on the protolith (e.g. calc-alkaline granitoid gives a positive anomaly as described by Villeneuve *et al.* (1993). Heterogeneous structure in the upper mantle beneath the GSLsz is suggested by both seismic and MT data, as described below.

4.1 Upper-mantle structure

MT data can be used to constrain the upper mantle structure, if low frequencies (long periods) are measured. A previous study of Northern Alberta identified an east dipping conductor extending into the upper mantle (Türkoğlu *et al.* 2009). The palaeogeotherm and the composition of the subcontinental lithospheric mantle (SCLM) beneath this region were studied through mantle xenoliths and xenocrysts retrieved from three of the 88–86 Ma Buffalo Hills kimberlites (K6, K11 and K14; Aulbach *et al.* 2004) and showed that the depth of the lithosphere–asthenosphere boundary (LAB) beneath this region was around 180 km. To the northwest of the GSLsz, the LAB depth on the southern edge of the Slave Craton beneath Yellowknife was estimated to be 250 km while the depth beneath the central craton was around 200 km (Jones *et al.* 2003). A loss of >20 per cent partial melt is recorded by spinel lherzolites and up to 60 per cent by the garnet harzburgites, which may be related to lithosphere formation. After formation of the lithosphere, several major metasomatic events occurred, followed by kimberlite magmatism at 88–86 Ma (Aulbach *et al.* 2004). These metasomatic events may have caused changes in the electrical structure of the SCLM, as illustrated by MT studies of the Slave craton (Jones *et al.* 2001; Jones & Craven 2004). The spatial relationship of the currently juxtaposed Slave craton and BHT raises the question of whether they were once part of a single larger craton (Aulbach *et al.* 2003). It could be possible to use resistivity structure to constrain the former geometry of crustal blocks on each side of the GSLsz. However a full discussion of this is beyond the scope of this paper.

The LITHOPROBE ABT used seismic and MT data to investigate the structure of the Alberta crystalline basement and underlying mantle lithosphere in order to define the extent of basement units in conjunction with potential field data and drill core samples. The results of these Alberta studies were interpreted by analogy with Cenozoic Plate tectonic models and with the Cenozoic India–Asia collision (Gibb 1978; Hoffman 1988, 1989). It has been inferred that crustal growth involved both terrane accretion (subduction-collision) and development of associated magmatic arcs (Pilkington *et al.* 2000; Ross & Eaton 2001). Boerner *et al.* (2000a, b) discovered two major conductors that were interpreted to be the remnants of convergent plate boundaries (the Red Deer conductor, RDC; and the Kiskatinaw conductor, KC). Although the ABT MT data crossed the GSLsz, it did not provide adequate coverage to reliably constrain the structure of the shear zone in NW Alberta.

The central GSLsz was studied with broadband MT data during the LITHOPROBE SNORCLE transect which imaged the shear zone as a crustal-scale high resistivity zone (>5000 Ω m) spatially correlated with an aeromagnetic low (Wu *et al.* 2002). Geoelectric strike directions determined from the MT data showed a strike direction of N30°E in the crust and N60°E in the upper mantle. A teleseismic study in the same area by Eaton *et al.* (2004) showed shear wave splitting directions in the crust of N30°E localized around the GSLsz, that overlaid a deeper, anisotropic layer with a fast direction of N60°E. The similar geoelectric strike directions and shear wave splitting directions suggests that a common mechanism may be responsible for both. While this may be true for the crust, in the mantle this may be a coincidence and this point is discussed in more detail later in the paper. Coincident gravity data showed that the GSLsz was characterized by a 10 mGal axial gravity high with a spatial wavelength of 30 km superimposed on a longer wavelength 12 mGal low (Hope & Eaton 2002). The density structure was consistent with the crustal model derived from receiver-function analysis that showed a Moho dipping inward toward the shear-zone axis and a mid-crustal zone with high *S*-wave velocity (Eaton & Hope 2003).

Recent teleseismic data collected at fourteen stations along a 150-km-long profile and recorded for 2–5 yr across the GSLsz provide a lithospheric-scale image of the MacDonald fault zone about 100 km northeast of the east arm of Great Slave Lake (Snyder & Kjarsgaard 2013). The long recording time and size of the array permitted receiver function analyses to image wedge-shaped features within

the upper mantle. The study also found no evidence of near-vertical suturing structures within the crust or the mantle and suggested that the Slave Craton keel had stabilized beneath the GSLsz as early as 2.0–1.9 Ga and that the GSLsz is an intraplate feature.

Despite the geophysical studies described above, there are still a number of features of the lithospheric structure of the GSLsz and northern Alberta, which are poorly understood. The magnetic signature of the GSLsz exhibits along strike variations, so it is likely that the resistivity also varies along strike. The central segment of the GSLsz was imaged by Wu *et al.* (2002) as a high-resistivity structure (>5000 Ω m), but it cannot be assumed that the shear zone is resistive along its entire length. Previous MT studies reported electrical anisotropy in a number of fossil shear zones (Weckmann *et al.* 2003), therefore close station spacing and high quality MT data are needed to reliably distinguish anisotropy from heterogeneity.

5 MT DATA USED IN THIS STUDY

This study uses a combination of previously collected data MT and new MT data that were collected to improve the spatial coverage. These data are located on the three profiles shown in Fig. 2 which are as follows:

SNORCLE: The northern line consists of 23 broad-band MT sites along the LITHOPROBE SNORCLE Transect Corridor 1A, which crossed the GSLsz, the Great Bear magmatic arc and Hay River terrane to the northwest of the shear zone, and the BHT to the southeast. A subset of this profile was previously analysed and modelled by Wu *et al.* (2002).

NAB: New long-period MT data were collected for this profile at 11 locations on a profile near Zama City in 2011 using NIMS instruments that recorded in the period band 1–10 000 s. At all stations two components of the horizontal electric field and three components of the magnetic field were measured for a duration of 3 weeks. Data were generally of good quality, but with cultural noise from oil and gas infrastructure at some stations. The impedance tensors and the geomagnetic transfer functions were estimated using standard robust processing (Egbert & Booker 1986; Egbert 1997) and remote reference data was used to minimize the effects of noise (Gamble *et al.* 1979).

ABT: The southern profile consists of 17 LITHOPROBE ABT long-period MT stations collected with LIMS instruments in the period range 20–10 000 s (Boerner *et al.* 2000a,b). Four additional stations were collected on this profile in 2011 using the NIMS instruments.

The southern two profiles cross the following terranes: Hottah terrane to the northwest of the GSLsz, Kiskatinaw Low, Chinchaga domain and BHT to the southeast of the shear zone (Fig. 2). It should be noted that the boundaries of these terranes are defined on the basis of aeromagnetic data.

6 DIMENSIONALITY AND DIRECTIONALITY ANALYSIS

Prior to the modelling of MT data, careful dimensionality and directionality analysis must be undertaken to determine if a 2-D or 3-D approach is required. MT signals penetrate to greater depths as their period increases so a study of different periods gives information about the depth variation of the resistivity structure. The results of the dimensionality analysis are shown in Fig. 4.

6.1 Strike direction from tensor decomposition

Tensor decomposition was used to estimate the strike directions (Groom & Bailey 1989) and the results shown in Fig. 4 were obtained using the algorithm of McNeice & Jones (2001). For all profiles, a strike close to the strike of the GSLsz is observed. At longer periods the SNORCLE profile has a strike N60°E while on the NAB and ABT profiles it is approximately N–S. The inherent 90° ambiguity was resolved by choosing the strike direction closest to the regional geological strike direction.

6.2 Phase tensor

Phase tensors were calculated using the method of Caldwell *et al.* (2004) and are shown in Fig. 4. Ellipticity indicates the degree to which the phase tensor is an ellipse, and the geographic orientation of the major axis. The principal axes of the ellipses are either parallel or perpendicular to the geoelectric strike in a 2-D resistivity structure. The colour of the ellipses represents the skew angle (β) which can be used to infer dimensionality, with values greater than 5° generally indicating 3-D effects. The small skew values shown in Fig. 4 indicates that 1-D/2-D structures are dominant in the study area. At short periods (10–64 s), the phase tensor orientations for the SNORCLE profile are roughly perpendicular to the strike of the GSLsz. At longer periods, the phase tensors are parallel to the strike of the GSLsz close to the shear zone. Several ∼90° changes in ellipse orientation occur along the profile and are marked with black dashed ellipses in Fig. 5. This may indicate the locations of interfaces between regions of different resistivity.

The phase tensors for the NAB and ABT profiles show similar patterns, especially at shorter periods (10–64 s). At sites near the GSLsz, the shape of the ellipses suggests a large phase split between the *xy* and *yx* impedances, which could be the result of 2-D resistivity structure or anisotropy. Additionally, the orientations of the phase tensor ellipses are approximately NW–SE. At a period of 320s, the phase tensors near the shear zone on the NAB and ABT profiles still show significant ellipticity, and the orientations become approximately N–S at longer periods. The sites at the eastern ends of the two profiles (located in the BHT) show phase tensors with weak ellipticity and orientations that are nearly E–W, and perpendicular to those of the western sites. A similar phenomenon can also be seen at a period of 1024 s, where all the NAB–ABT sites show weak ellipticity.

6.3 Induction vectors

Induction vectors are computed from the vertical magnetic field components and contain information about the dimensionality of the subsurface resistivity structure. They reverse direction above a conductor, and are sensitive to horizontal changes in resistivity. In a 1-D case the induction vectors have zero length, while in 2-D and 3-D the vectors point at conductors when plotted in the Parkinson convention (Parkinson 1962). In a 2-D situation, the induction vectors will be orthogonal to the strike direction, allowing the 90° ambiguity in geoelectric strike to be addressed.

6.3.1 Short period (T = 10 s)

Induction vectors on the ABT and NAB profiles are quite small (∼0.05) and show no consistent direction. These two profiles are located in northern Alberta where the WCSB is ∼1 km deep. This

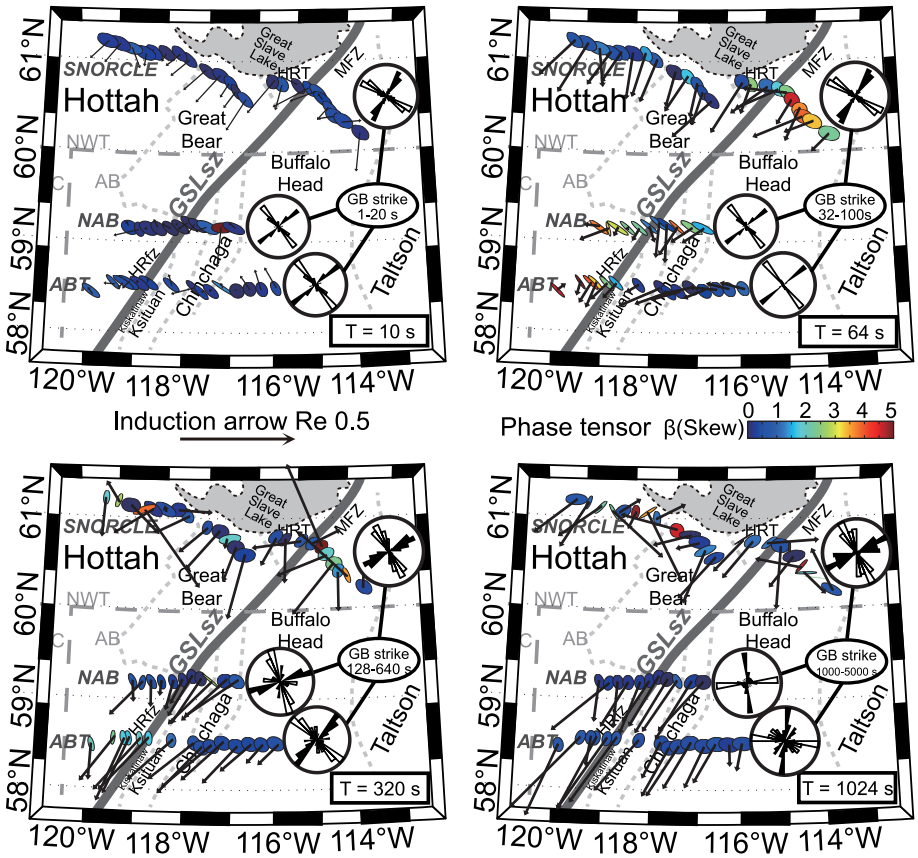

Figure 4. Geoelectric strike direction, phase tensor and real induction arrows for periods of 10, 64, 320 and 1024 s. Strike direction are shown as rose diagram at the eastern end of each profile, and the black-white sectors illustrate the 90° inherent ambiguity. Phase tensor ellipses are shaded according to skew value. The induction vectors are plotted in the Parkinson convention, pointing towards conductors.

layer has limited horizontal variations in resistivity, consistent with the small induction vectors. In contrast, the vectors at 10 s on the SNORCLE profile consistently point southwest, indicating the location of a conductor. This could be either the southwesterly thickening of the WCSB or a low resistivity anomaly associated with the shear zone.

6.3.2 Intermediate period (T = 64 s)

SNORCLE induction vectors have similar directions to those at 10 s but their amplitudes are greater. However, greater differences in the length and direction of the induction vectors are observed on the ABT and NAB profiles. The enhanced lengths may indicate a large conductive feature, and the large (∼80°) deflection of the vectors near the shear zone on both profiles, may indicate a NE-SW trending conductor. All the induction vectors appear to show the superposition of a component pointing to southwest, parallel to the shear zone and a component orthogonal to the GSLsz. The parallel component is inferred to be due to the low resistivity of the WCSB, while the orthogonal component may indicate that the GSLsz is a conductor that deflects the induction vectors, and may even cause a reversal.

6.3.3 Long period (T = 1024 s)

The induction vectors on the ABT and NAB profiles show a consistent orientation pointing to southwest with large magnitudes. Major crustal and upper mantle conductors were reported beneath the Canadian Cordillera (Majorowicz *et al.* 1993; Jones & Gough 1995; Soyer & Unsworth 2006; Rippe *et al.* 2013), and could potentially explain these induction vectors. However 3-D MT modelling has not been able to reproduce this effect.

6.4 Summary of dimensionality and directionality

Tensor decomposition, phase tensor ellipses and skew values all give evidence for an approximately 2-D resistivity structure. A strike of N45°E is consistent with the data in the period range 1–300 s, while at longer periods (300–1000 s) a strike direction of N60°E is preferred. The phase tensors show a more complex geometry compared to that inferred from the tensor decomposition. The induction vectors are not perpendicular to the regional strike direction, and suggest a 3-D resistivity structure. External support of the strike directions comes from the SKS splitting directions determined from the coincident SNORCLE teleseismic data of Eaton *et al.* (2004). This suggested a two-layer seismic anisotropic model, with directions N30°E and N60°E for the upper and lower layer respectively. These directions are somewhat consistent with the strike directions derived from the MT data (N45°E for the crust and N60°E for the mantle). It is clear that the crustal strike directions derived from MT and seismic data may have a common origin i.e. highly sheared mylonites. However, in the upper mantle, especially under dry conditions, it is not clear if a single physical mechanism can explain both strike directions.

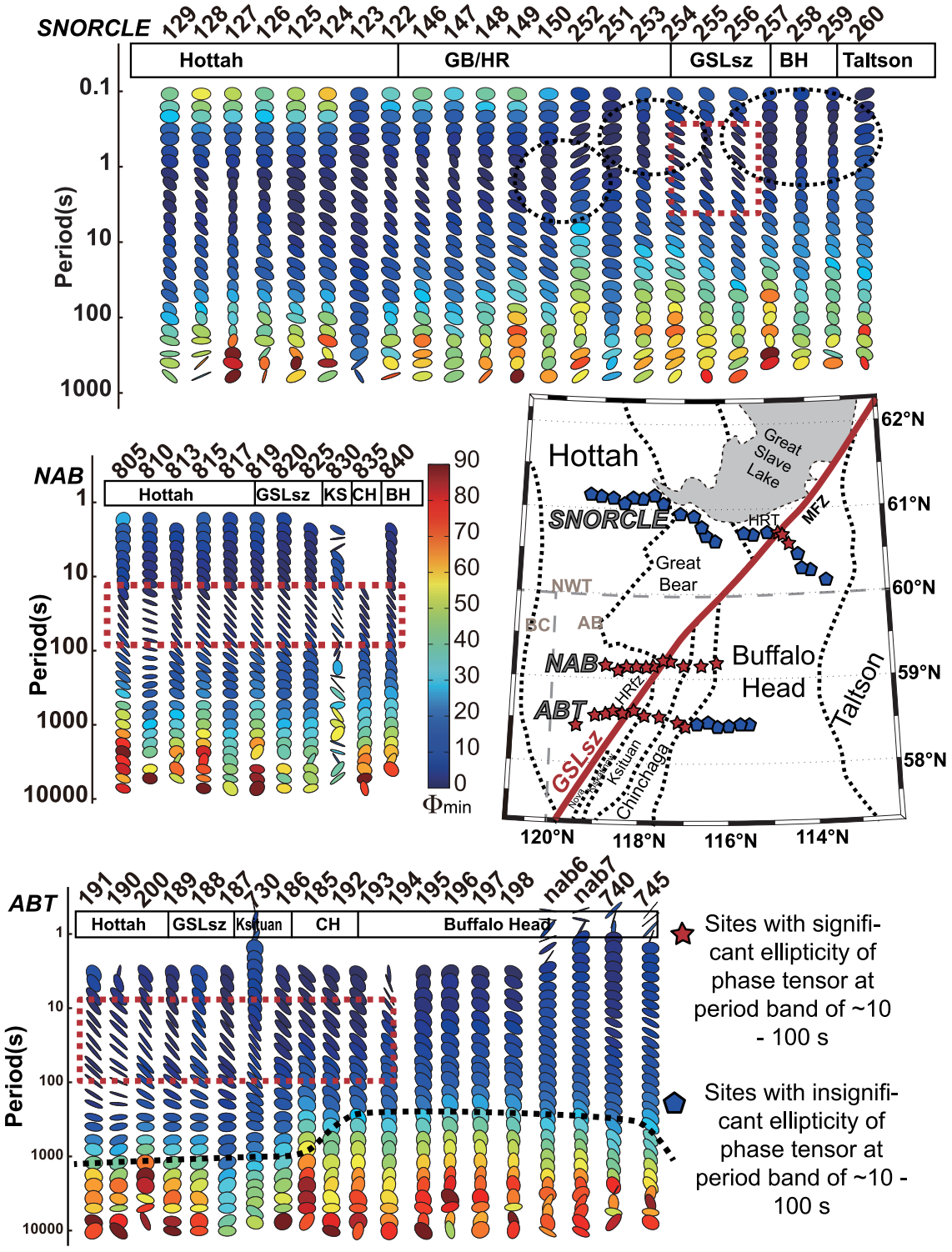

Figure 5. Phase tensor ellipse pseudo-section for the 3 profiles. The colour used to fill the ellipses shows the minimum phase Φ_{min}. The stations are grouped according to whether they show obvious phase split in the 10–100 s band. The red dashed boxes highlight the phase tensors showing obvious polarization. Note that the SNORCLE data were collected in a shorter period band than the NAB and ABT profiles. The dashed line on the ABT profile indicates the resistivity interface inferred from the significantly decreased Φ_{min} values.

7 EVIDENCE FOR ELECTRICAL ANISOTROPY

Electrical anisotropy is not unexpected in a zone of deformation such as the GSLsz. Thus additional analysis was undertaken to see if the MT data requires an anisotropic resistivity structure. Characteristics of MT data that can be used to identify electrical anisotropy include: (i) apparent resistivity and phase differences between two orthogonal polarization directions, (ii) phase tensors and (iii) induction vectors. In this section, the GSLsz MT data are investigated for evidence of electrical anisotropy.

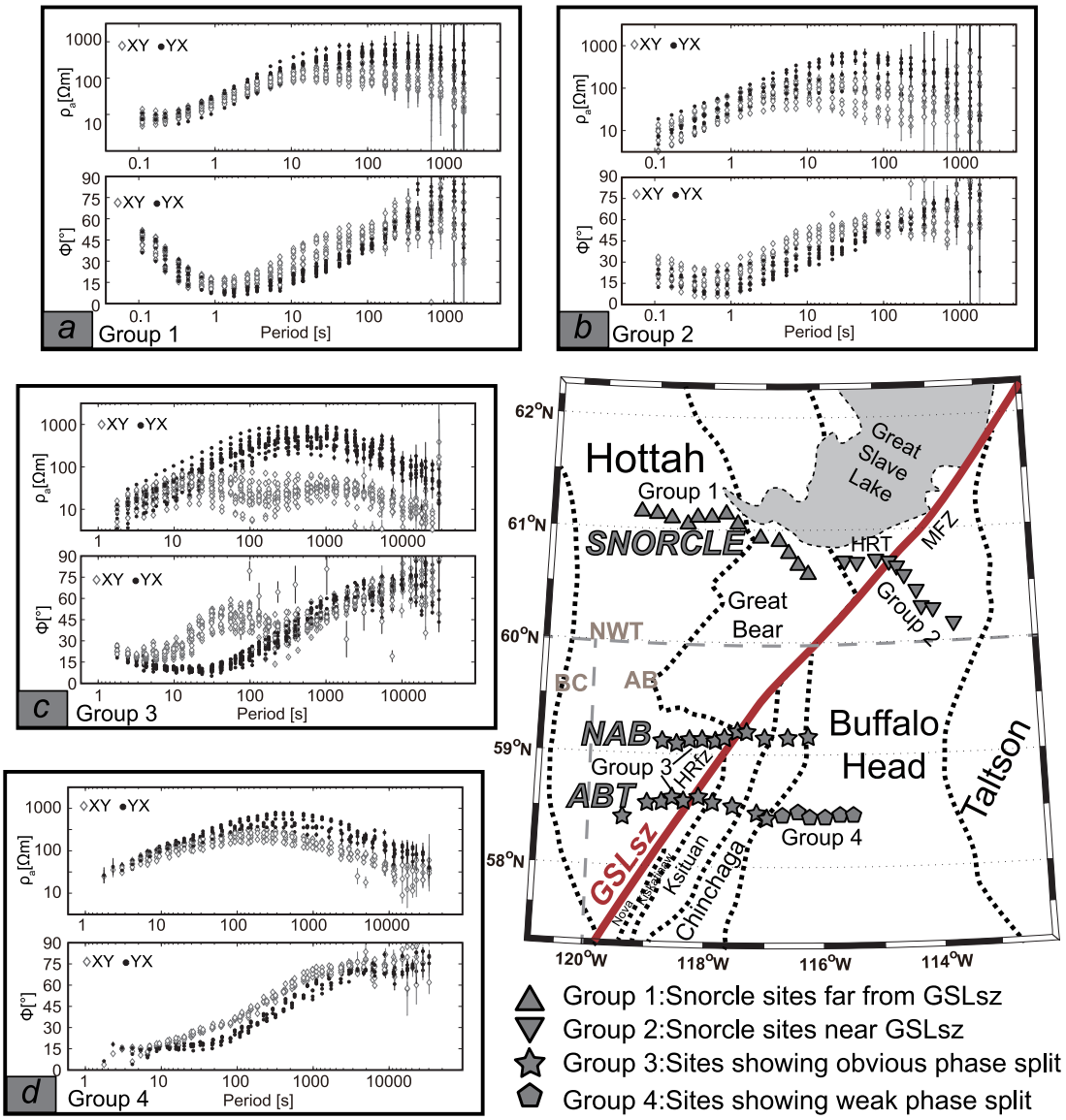

Figure 6. Apparent resistivity and phase curves in a N40°E co-ordinate system, divided into groups according to the shape of curve.

7.1 Evidence for anisotropy from phase splits

The first stage in looking for indications of anisotropy is to determine if there are distinct areas with characteristic geoelectric strike direction, phase tensor, apparent resistivity and phase curves. For classification, the stations were divided into the four groups shown in Figs 6 and 7.

7.1.1 SNORCLE profile

These data were divided into Groups 1 and 2 on the basis of the shapes of the sounding curves in Fig. 6 and show no evidence of anisotropy, with phase splits less than 10° between the TE and TM modes. Several isolated zones with high phase differences may indicate local 2-D heterogeneity as opposed to anisotropy.

7.1.2 NAB and ABT profiles

Group 3 stations on the NAB and ABT profiles show a strong phase split that reaches 35° in the period band of 10–300 s (Figs 6 and 7). These stations are located in both the GSLsz and all adjacent terranes, except for the BHT. This type of phase split at multiple stations can be caused by an electrically anisotropic layer (Kellett *et al.* 1992; Eisel & Bahr 1993; Jones *et al.* 1993; Eisel *et al.* 2001). Group 4 stations on the ABT profile show a minimal phase split and are located within the BHT. Thus we infer that an anisotropic layer may exist beneath Group 3 stations, and is absent beneath Group 4 stations. Heterogeneity could be an alternate explanation for the phase splits, but when combined with the other evidence, anisotropy is the preferred explanation. One common characteristic of all the MT stations in northern Alberta is that the phase values increase at periods greater than 100 s and remain above 45° at periods greater than 500 s (Fig. 7). This indicates a conductor at depth, as shown in previous studies to correspond to upper mantle depths (Türkoğlu *et al.* 2009).

7.2 Evidence for anisotropy from phase tensors

Phase tensors may also provide evidence for the presence of electrical anisotropy. Heise *et al.* (2006) showed that for a 1-D resistivity

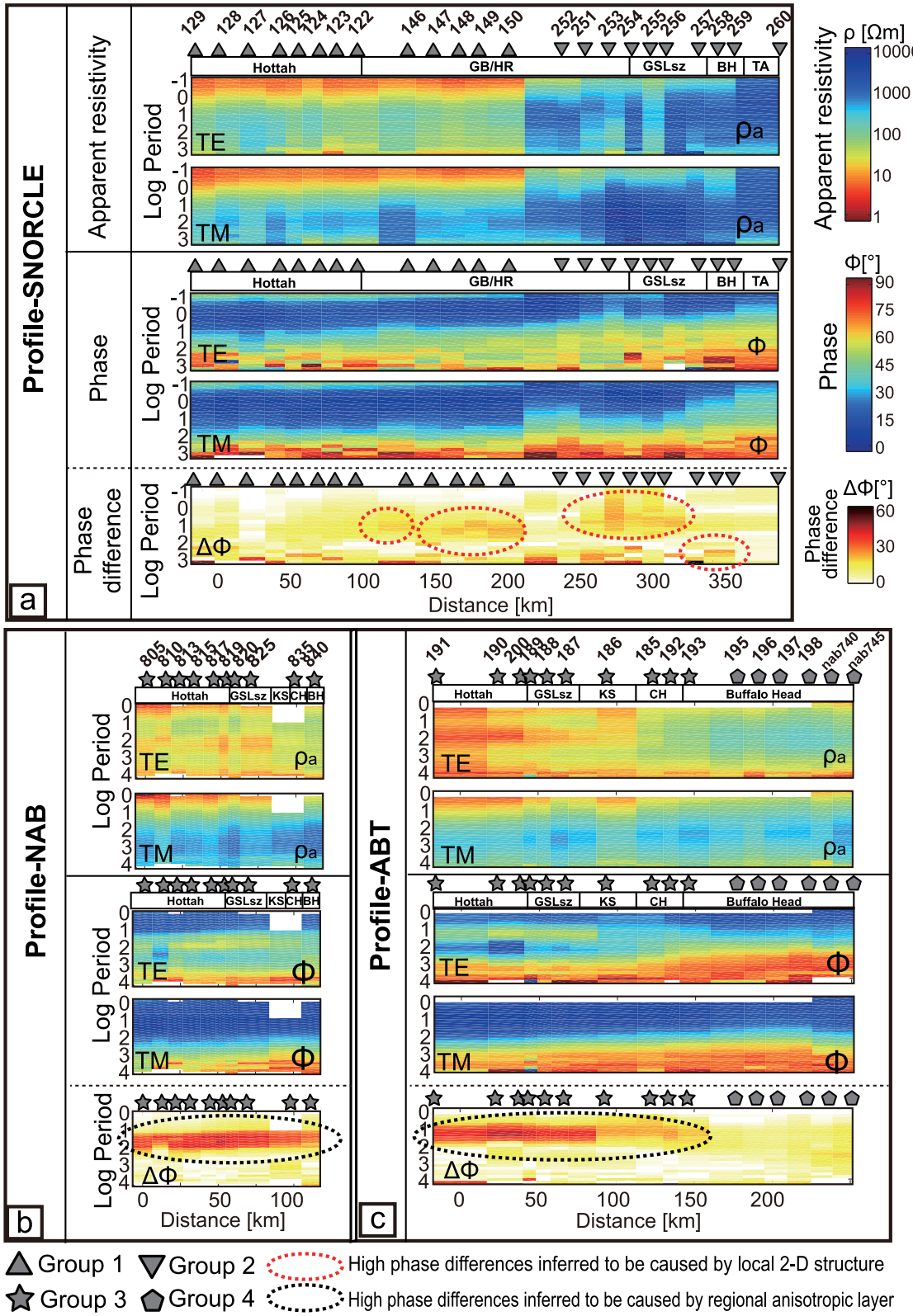

Figure 7. Pseudo-sections of the observed impedance tensor data for the SNORCLE, NAB and ABT profiles in a N40°E co-ordinate system.

model, a phase split can be produced by the conductivity change at the interface between isotropic and anisotropic layers. The maximum phase difference is determined by the conductivity contrast between the principal conductivities of the anisotropic layer and the isotropic layer's conductivity. Phase tensor ellipse pseudo-sections are shown for the three profiles in Fig. 5. The colour fill shows the value of Φ_2 which is the geometric mean of the maximum and minimum phases. Higher values of Φ_2 indicate increasing conductivity with depth and vice versa. Some stations on the NAB profile show spatially consistent ellipticity features in the period band 10–100 s

and are identified with a red star/box on the map/pseudosection in Fig. 5. The major axes of the ellipses are oriented N45°W, perpendicular to the regional strike direction. A similar pattern is observed in the western part of the ABT profile. These consistent directions could be caused by either 2-D electrical structure or an intrinsically anisotropic layer. If the constant phase splits over a large area were caused by a single 2-D electrical heterogeneity, an unrealistically large structure would be required. Thus, 2-D electrical heterogeneity can be probably excluded, and anisotropy is the preferred explanation. In contrast, the stations on the eastern ABT profile (in the BHT) show weak ellipticity in the same period band (10–100 s), indicating a 1-D structure in this area and the absence of anisotropy.

The phase tensor pseudo-section of the SNORCLE profile shows a totally different pattern compared to the two southern profiles. The orientation of the phase ellipse changes twice along the profile (Fig. 5, marked by black circles). Since a 90° flip of the phase tensor orientation can be caused by a conductive interface, this suggests the presence of 2-D heterogeneity beneath the SNORCLE profile. The stronger ellipticity of the phase tensors at stations near the GSLsz (254, 255 and 256), may indicate a significant conductivity contrast associated with the shear zone. In contrast, the consistent phase tensor orientations on the NAB and ABT profiles provides evidence for the presence of crustal anisotropy, as opposed to heterogeneity. At short periods at most stations, Φ_2 is less than 30° indicating an increasing resistivity with depth. This likely corresponds to the transition from the near-surface conductive sedimentary layer to underlying crystalline basement.

7.3 Induction vectors–evidence for anisotropy

Heise & Pous (2001) showed that induction vectors can be influenced by electrical anisotropy. Their direction will depend not only on the regional strike direction, but also the strike of the intrinsic anisotropy, if non-parallel to the regional geoelectric strike. In a general case, the induction vector directions are generally not perpendicular to either the regional strike direction or the anisotropic strike. This situation can be observed in the GSLsz data since the induction vectors are not perpendicular to the strike direction determined from tensor decomposition and the phase tensor (Fig. 8). Note that the amplitudes of the induction vectors in the period band of 10–100 s for the NAB and western part of ABT profile are quite small (most are less than 0.1). In this period band, conspicuous phase splits and phase tensor ellipticity can be observed on both these profiles (Figs 5–7). The lack of correlation between the phase splits and the induction vectors for the GSLsz data, means that a lateral conductivity gradient might be ruled out as a cause of the phase split. In addition, constant phase splits over an extended area, as depicted in the phase difference pseudo-sections in Fig. 7 suggests that the phase splits are not caused by a number of discrete conductors. This leaves anisotropy as the most reasonable interpretation.

Another relevant feature of the NAB and ABT profiles is the induction vector direction in the period band 100–10 000 s as shown in Fig. 8. A consistent orientation of ∼S60°W can be observed, which is nearly parallel to the regional strike direction (N45°E). A 2-D structure should generate induction vectors perpendicular to the regional strike. However the induction vectors may be deflected if an anisotropic layer is present (Pek & Verner 1997). The cause of the deflection was suggested to be that the currents flowing in the isotropic conductor escape into the anisotropic layer and then flow in the most conductive direction in that layer. The vertical magnetic field is generated by the change in current direction. This deflection could also be due to 3-D isotropic resistivity structure (Heise & Pous 2001). The pattern of long period induction vectors beneath the BHT also point SW, and in this area there are no signs of anisotropy from other indicators. This may indicate that large scale 3-D structures are causing the SW orientation of the induction vectors. Compared with the other two profiles, the SNORCLE profile shows a more scattered pattern of induction vector directions. This may be caused by small scale (3-D) resistivity structures. However, the long-period MT data is of lower quality on this profile and further discussion of the data is not warranted.

7.4 Summary of anisotropy analysis

From the analysis described above, an anisotropic layer is located in the vicinity of the GSLsz on both the ABT and NAB profiles. In contrast, there is weak or no anisotropy on the SNORCLE profile and in BHT far from the GSLsz. Anisotropy can be inferred qualitatively from the analysis above, and detailed characterization requires inversion—as described in the following section.

8 2-D AND 3-D ISOTROPIC INVERSIONS

8.1 2-D isotropic inversion

8.1.1 SNORCLE

The TE, TM and tipper data were inverted using the algorithm of Rodi & Mackie (2001) in a N40°E co-ordinate system. Error floors of 20 per cent for apparent resistivity, 5 per cent for phase and 0.04 for tipper were used. The inversion was repeated for a range of regularization parameters to explore the trade-off that occurs as the requirement for a spatially smooth model was varied. When plotted as an L-curve, it was found that the preferred value of the trade-off parameter τ, was 3. After 200 iterations the data were fit with an rms misfit error of 1.743. Evidence of static shifts can be observed in the apparent resistivity curves at some sites (e.g. site 256). Thus, the inversion included estimation of static shift coefficients shown in Fig. 9(b). A coefficient of 0 indicates a station that was not affected by static shift, while the value 1 indicates a shift of 10. The rms misfit reduced to 1.654 when the inversion was allowed to compute static shift coefficients. The fit at four sites are shown in Fig. 9(d) and the measured data are generally well fit. The fact that the main model features do not change significantly when different control parameters were used indicates the robustness of the inversion models. The main model features in Fig. 9(a) are similar to those of Wu *et al.* (2002) and are labelled as conductors C_a, C_b and C_c and resistors R_a, R_b, R_c and R_d. Only features C_c, C_d and R_d are relevant to this paper. R_d is a 25 km wide subvertical resistive zone (>5000 Ω m) located beneath the GSLsz and flanked by C_c and C_d. Wu *et al.* (2002) suggested that R_d was due to the presence of high resistivity mylonites formed by ductile shearing.

8.1.2 NAB and ABT profiles

The same inversion algorithm and parameters were used as for the SNORCLE profile. A τ value of 3 was chosen for the inversion of these two profiles. Error floors of 20 per cent for apparent resistivity and 5 per cent for phases were also used. It should be noted that data on these profiles are long-period MT data, while the SNORCLE data were broadband MT data. The induction vectors show an unexpected NW direction which is not perpendicular to the regional

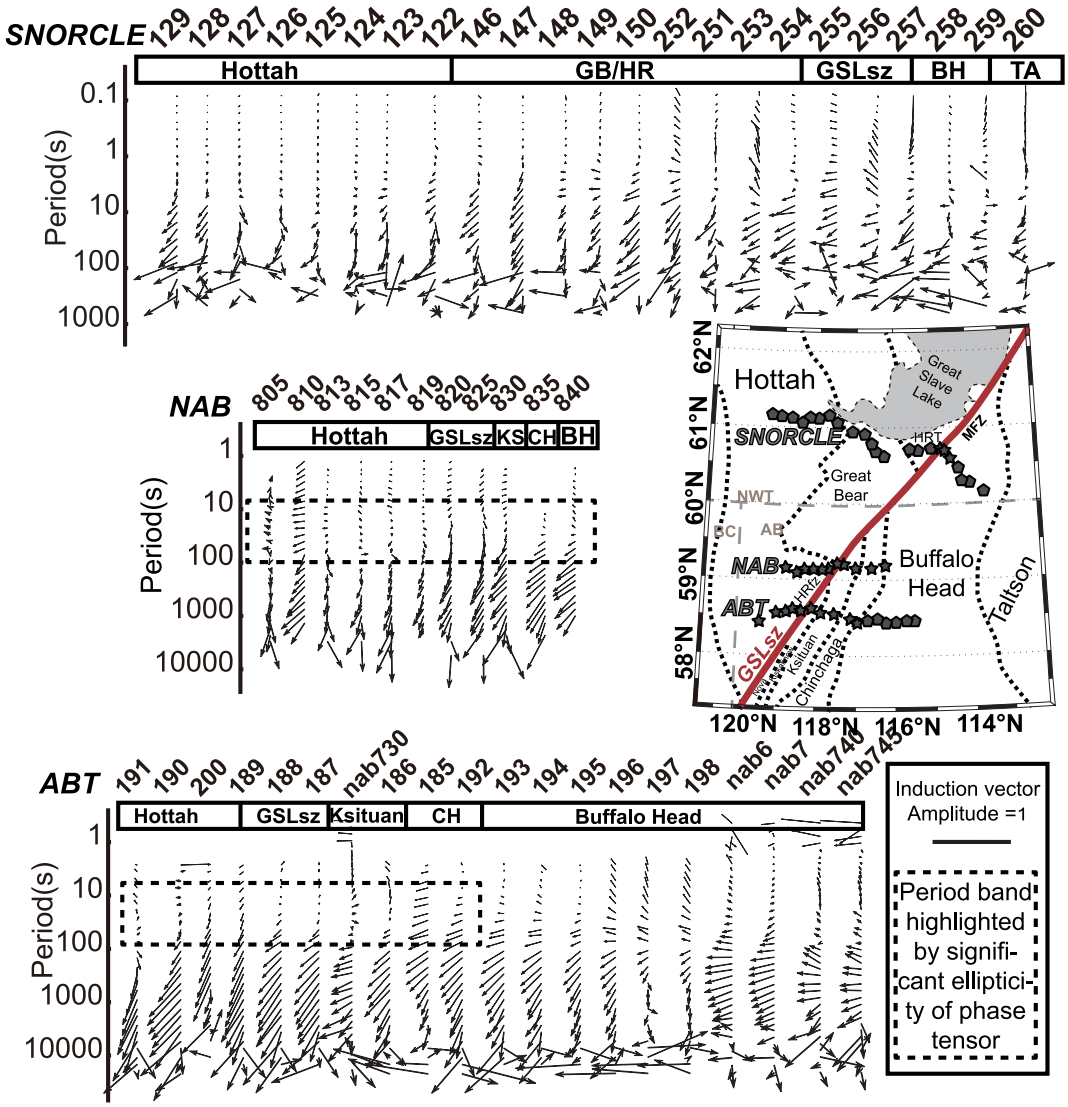

Figure 8. Real induction vectors plotted in the Parkinson convention (pointing towards conductors) plotted on the three profiles. The black dash boxes on the profile ABT and NAB highlight the period band with obvious phase tensor polarization shown in Fig. 3. The lack of correlation between induction vector direction and phase tensors orientation supports the hypothesis that an anisotropic layer is present.

strike direction, so as with the SNORCLE data, a relatively large error floor of 0.04 was used for the tipper. rms misfits of 1.611 and 1.857 were obtained for the NAB and ABT profiles, respectively. The upper panels of Fig. 10 show the 2-D inversion models for the NAB and ABT profiles, while the lower panels show corresponding slices of the 3-D inversion models discussed in the next section. A thin conductive layer can be seen in both models at shallow depths within a few km of the surface, and is attributed to the sedimentary rocks of the WCSB.

On the ABT profile, three major crustal conductors can be discerned. Along the profile from NW to SE, conductor C_1 is located beneath the Hottah terrane, with resistivity values below 10 Ω m extending from surface to a depth of ∼25 km. The geometry of this conductor is only constrained by 2 widely spaced MT sites. A second, eastward dipping conductor (C_2) can be observed on the western margin of the GSLsz at mid to lower crust depths (10–35 km). As is always the case in MT, the base of this conductor cannot be well resolved. The third conductor (C_3) is located beneath the boundary of the GSLsz and the Ksituan terrane extending from the uppermost sedimentary basin to a depth of ∼20 km, which is at a similar location and depth compared to the KC (Kiskatinaw conductor) reported by Boerner *et al.* (2000a,b). Finally, C_4 is an upper mantle conductor located zone beneath the BHT. This feature was previously reported by Türkoğlu *et al.* (2009) and believed to be an upper mantle associated with a prior subduction event, perhaps identified as the source of carbon for the diamonds found in the Buffalo Head Hills. The whole upper mantle beneath this profile is conductive at depths greater than 120 km (C_5) and may also related to prior subduction events. Resistive zones R_1, R_2, R_3 and R_4 are also defined in Fig. 10. It is significant that almost all the resistivity features of the 2-D ABT model can be observed in the 2-D NAB model, with similar locations and depths. This gives evidence for a 2-D regional resistivity structure.

8.2 3-D inversion for the NAB and ABT profile

To ensure that the 2-D inversion models are robust, a 3-D inversion was applied to the NAB and ABT profiles. The impedance and tipper data were inverted in geographic coordinates using the 3-D inversion algorithm of Siripunvaraporn *et al.* (2005). The initial

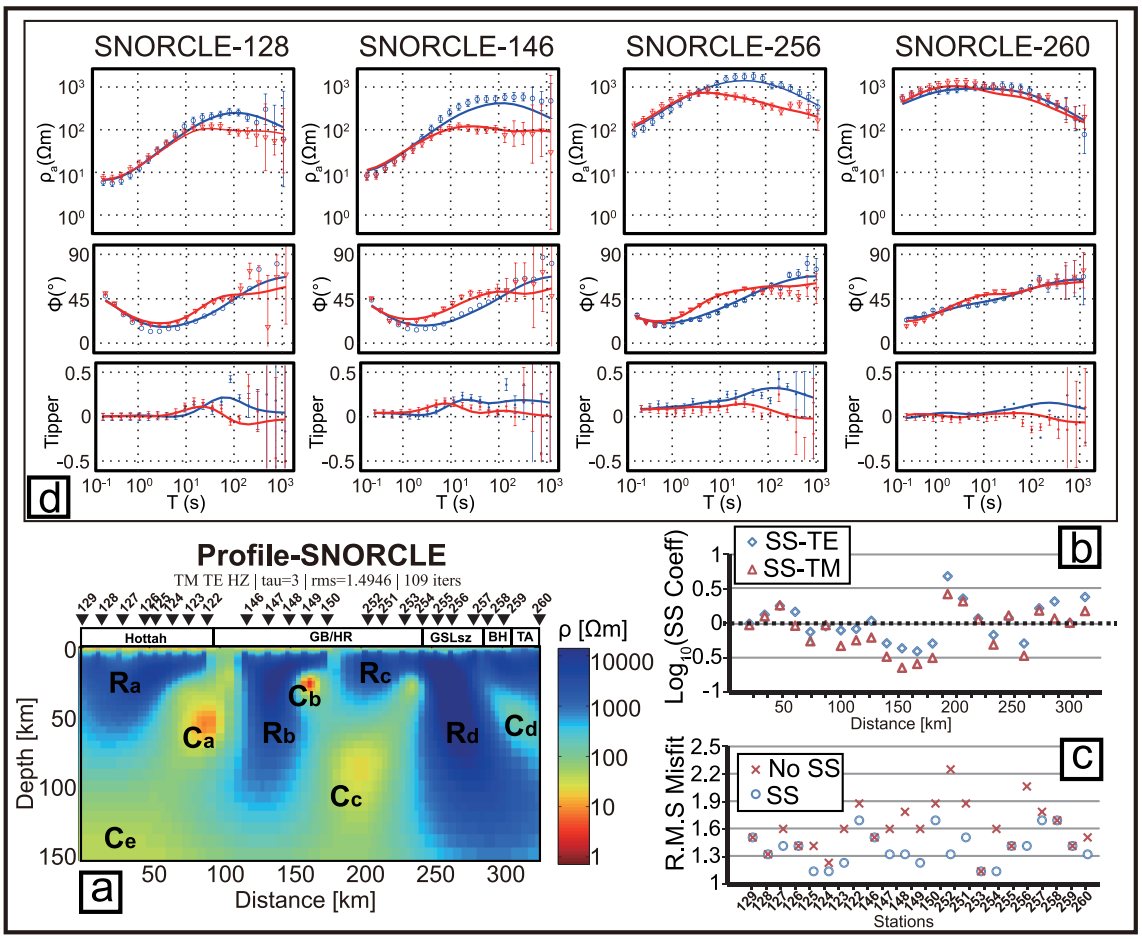

Figure 9. 2-D isotropic inversion of the SNORCLE profile. (a) Inversion model. GB, Great Bear; HR, Hay River terrane; BH, Buffalo Head; TA, Taltson. (b) Calculated static shift coefficients estimated by the inversion. SS, Static shift. (c) Comparison of rms misfits between inversions with/without static shift estimation.

3-D mesh grid is shown in Fig. 11(a) and the full impedance tensor and tipper data were inverted. Error floors of 15 per cent of the absolute values of the off-diagonal impedances were applied to all elements of the impedance tensor and 0.04 for tipper were used. In this inversion, the time step and three length scale values are used to control the spatial smoothness of the resistivity model. Values of 10, 0.1, 0.1 and 0.1 were chosen to give the best trade-off between resistivity model smoothness and data misfit. After 17 iterations, an acceptable rms misfit of 1.57 was achieved. Fig. 10 shows slices of the 3-D model, allowing a comparison with the 2-D inversions. Resistivity features observed in the 2-D models for the NAB and ABT profiles can also be seen in the 3-D model. However, the conductors in the 2-D and 3-D models, do not occur at exactly the same depths or have the same absolute resistivity values. This behaviour has previously been reported in 3-D inversions (Bertrand *et al.* 2012a,b; Tietze & Ritter 2013). For example, conductor C_4 is not as conspicuous in the 3-D inversion model as it was in the 2-D inversion. The conductors C_3 and C_4 are distinct in the 2-D inversion model while in the 3-D inversion model they are merged into a single conductor extending from 20 km to a depth greater than 200 km. The conductive zone between C_3 and C_4 (40–70 km) in the 3-D model probably may be an artefact caused by the relatively coarse vertical spacing of the 3-D inversion mesh. It should be also noted that other factors mean that a comparison of the 2-D and 3-D inversions should be made with care. The 3-D inversion used a smaller data set and a coarser grid than the 2-D inversion owing to computer memory and speed limitations and this can limit the complexity that can be reproduced in the model. On the other hand, the 3-D inversion of a profile may be more reliable than a 2-D inversion if the MT data exhibit some non 2-D features. However, in this case it should be noted that, overall, the two inversion methods give similar resistivity models.

In order to compare the fits of the 2-D and 3-D inversions, the modelled data of the 3-D inversion were rotated to the same direction as the 2-D inversion (Fig. 11). The rms values are shown in Fig. 11(b) and both are generally acceptable on both the ABT and NAB profiles and in the range 1–2.5. However, on the ABT profile, the 2-D inversion shows a significantly higher rms misfit, especially for stations east of the GSLsz. The consistently low rms misfit level on the NAB profile may indicate this area is more 2-D than the ABT profile. The 3-D model used larger model cells, thus giving lower resolution than for the 2-D models. Therefore detailed analysis and interpretation focused on the 2-D inversion models.

8.3 Anisotropic electrical features on isotropic inversion models

Conductors appear at similar locations on both the ABT and NAB profiles, although the shapes are quite different. On the shorter NAB profile, the 2-D and 3-D models show more differences than on the ABT profile. It is not clear if these features can be correlated

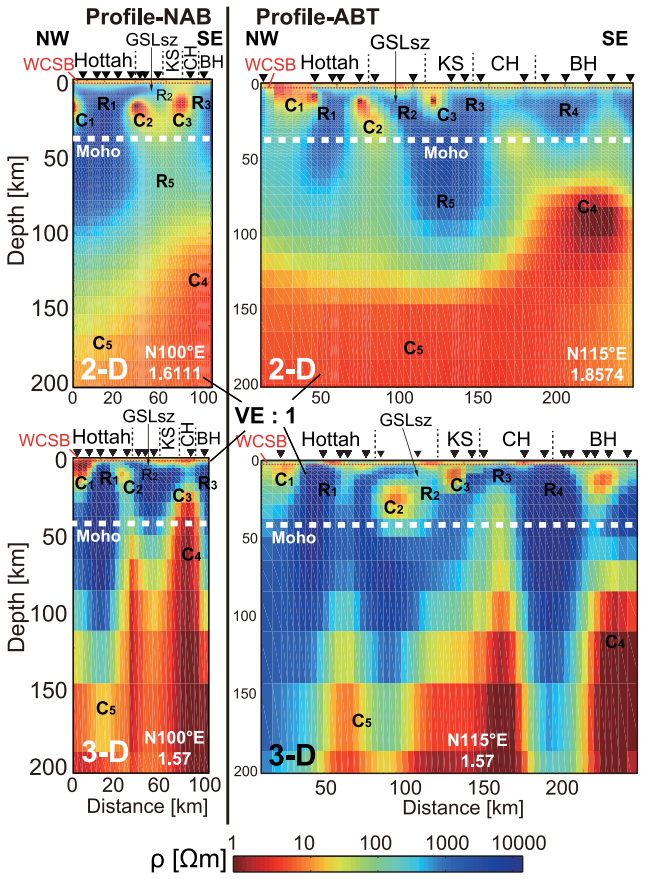

Figure 10. 2-D and 3-D isotropic inversion models for the ABT and NAB profiles. Models plotted with 1:1 vertical exaggeration. Labels for geological structures are the same as in Fig. 7.

between profiles. A number of previous MT studies of ancient orogens have produced resistivity models characterized by a series of conductive blobs (Jones *et al.* 1993, 1997, 2005; Jones 2006; Boerner *et al.* 2000a,b; Brasse & Soyer 2001). Numerical studies by Heise & Pous (2001) have shown that this type of structure can be an artefact that is generated when anisotropic MT data are inverted with a 2-D isotropic inversion. Thus the inversion models in Fig. 10 could support the hypothesis that electrical anisotropy is present in the crust beneath the NAB and ABT profiles.

9 ANISOTROPIC INVERSION

9.1 2-D anisotropic inversion for the profile ABT

The ABT profile was inverted using the anisotropic version of the Rodi & Mackie (2001) inversion. In this inversion, the resistivity of each cell is not completely general, but represented by the three diagonal components of the resistivity tensor, that is parallel/perpendicular to the strike direction (ρ_{xx} and ρ_{yy}) and in the vertical direction (ρ_{zz}). The same data and control parameters were used in both the anisotropic and isotropic inversions. An additional parameter is needed in the anisotropic inversion to control the degree to which differences are allowed between ρ_{xx}, ρ_{yy} and ρ_{zz}. This term is called the anisotropic tau (τ_{anis}) and high values will force the model to be isotropic with $\rho_{xx} = \rho_{yy} = \rho_{zz}$ while $\tau_{anis} = 0$ imposes no constraints on the three components.

ABT profile inversions were run using three different values of τ_{anis} (0.1, 0.5 and 1) and the results are shown in Fig. 12. In each column, the three models show the resistivity in x, y directions and the ratio of ρ_{xx} and ρ_{yy} is also plotted to show the degree of anisotropy. As expected the differences between ρ_{xx} and ρ_{yy} become greater as τ_{anis} decreases. As with the isotropic inversion, a series of discrete conductors are observed, and they have the lowest resistivity in the strike direction. The number and location of conductors changes with τ_{anis} but they clearly define an east dipping feature. It is likely that the individual conductors are artefacts and the true structure could be a continuous, anisotropic layer. Note that the rms misfit decreases with τ_{anis} which is expected since the anisotropic inversion has more degrees of freedom (Fig. 12c). While the lower rms misfit does not prove that an anisotopic model is required, it supports this hypothesis, especially combined with other indications of anisotropy presented earlier in the paper. In contrast, the upper-mantle conductor below a depth of 75 km exhibit no differences between ρ_{xx} and ρ_{yy}, which can be represented as an isotropic feature. Although the resolution of the model at this depth is still uncertain, it is inferred that the upper mantle is isotropic.

9.2 Anisotropic inversion for the profile SNORCLE and NAB

Inversion models for the NAB and SNORCLE profiles with anisotropic $\tau = 0.5$ are shown in Fig. 13. This values represents an inversion that allows a moderate amount of anisotropy. The NAB anisotropic inversion is similar to the western part of the ABT anisotropic inversion (Fig. 13a). Combined with the similar shapes of apparent resistivity and phase curves (Fig. 6) and the phase splits (Fig. 7), it is reasonable to believe that the similarity of the mid-lower crustal resistivity anisotropic features shown on the models of the two profiles may be caused by the same electrical anisotropic structure. The SNORCLE inversion also shows regions of anisotropy, again with the lowest resistivity in the strike direction. In contrast to the NAB/ABT profiles, the low-resistivity features are separated by significant distances, so large-scale electrical anisotropy may be ruled out. This supports observations from the phase tensors that the geoelectric structure of this region is characterized by a 2-D isotropic structure. This is consistent with the interpretation of Wu *et al.* (2002).

10 SUMMARY OF INVERSIONS

When the various 2-D and 3-D inversions are combined, significant spatial variations in the resistivity structure of the study area can be observed. Specifically, a high resistivity zone is detected beneath the GSLsz on all three profiles, that is feature R_d for SNORCLE profile, R_2 for the NAB and ABT profiles. These high resistivity zones are located between conductors (R_d between C_c and C_d, R_2 between C_2 and C_3). However, the width and depth of the resistive zones differs. In addition, the shapes of the resistive zones and crustal structure surrounding them are different.

The feature R_d in the SNORCLE profile inversions is a wide (>25 km) resistive zone extending from the surface to upper mantle depths (>150 km). In contrast, the 2-D inversion of the NAB profile shows a resistive core bounded by discrete conductors on each margin of the GSLsz, especially in the anisotropic 2-D inversion. The ABT profile shows a set of discrete conductors and the longer profile shows that this is part of an eastward dipping conductor, as reported by Türkoğlu *et al.* (2009). There is good evidence that this conductor is anisotropic, and it is significant that it extends across the GSLsz. It cannot be determined if the GSLsz is actually located between low resistivity features and it should be noted that when

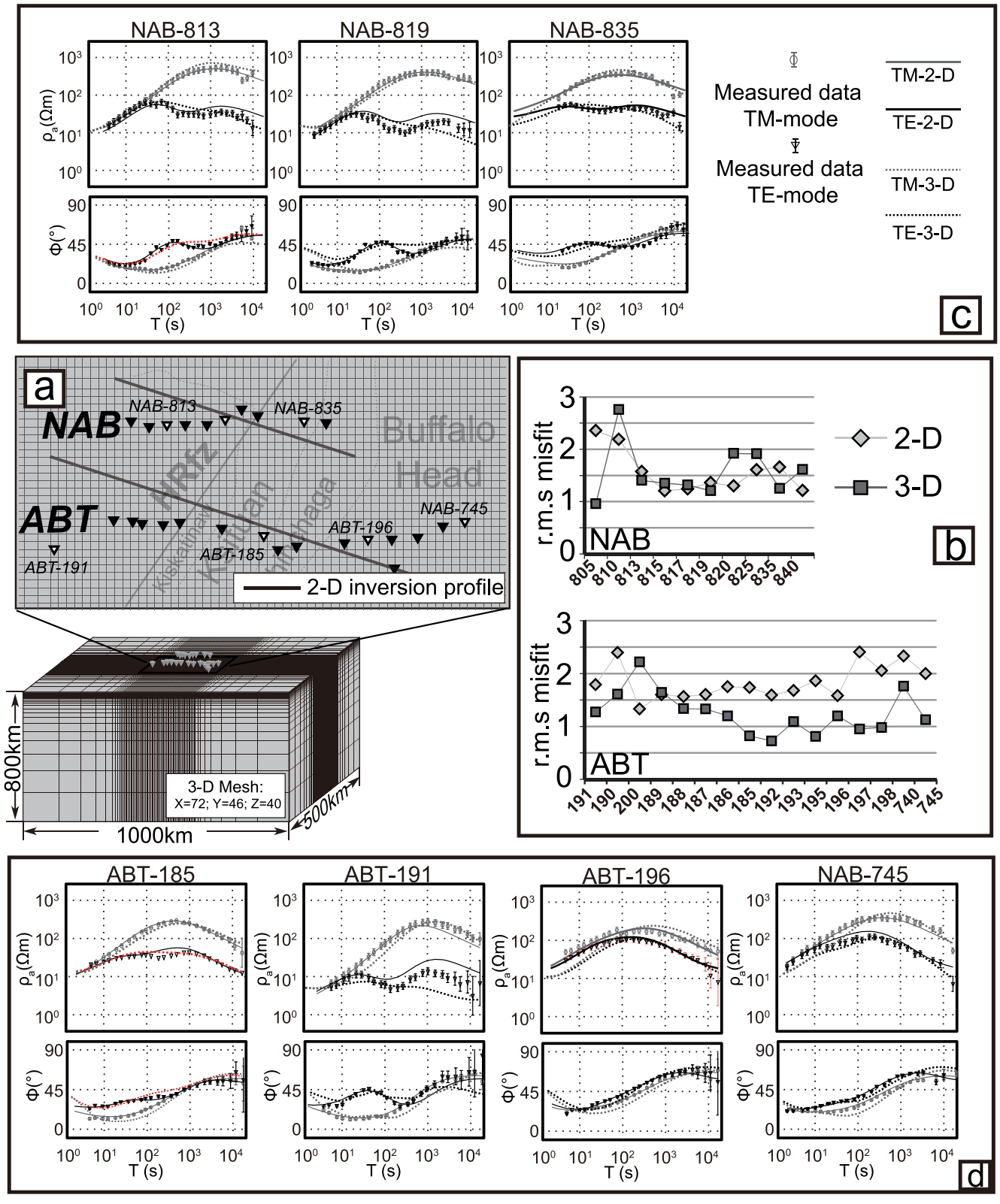

Figure 11. (a) The initial model for the 3-D inversion. (b) Comparison between the rms misfits of 2-D and 3-D inversion. (c)–(d) Comparison of the resistivity and phase curve fits between 2-D and 3-D inversion. Note that the 3-D inversion results are rotated into the regional strike direction for comparison with the 2-D inversion results.

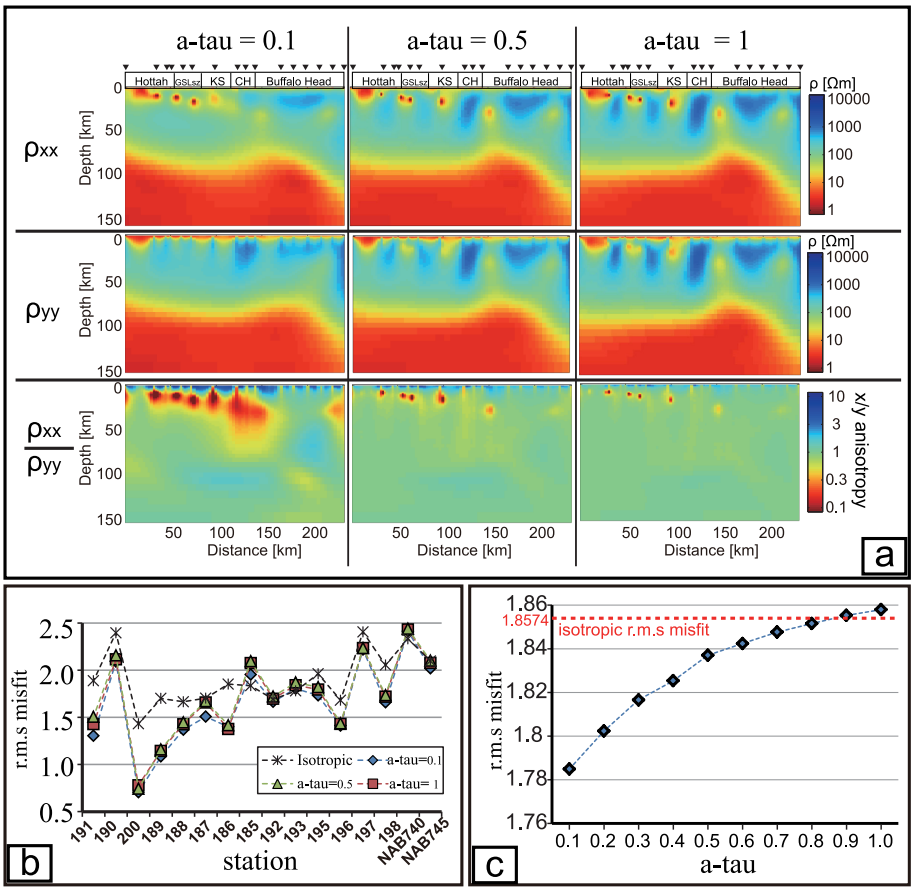

Figure 12. (a) 2-D anisotropic inversion models for the ABT profile (b) rms misfit comparisons between isotropic inversion and anisotropic inversion (c) effect of using different anisotropic τ values. Note that ρ_{xx} denotes the resistivity along strike while ρ_{yy} denotes the resistivity across strike.

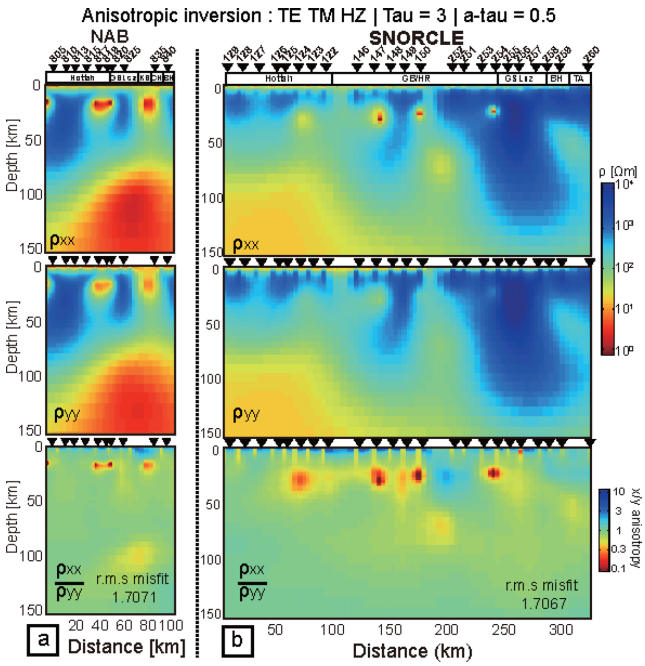

Figure 13. Anisotropic inversion models for the NAB and SNORCLE profiles. Note that ρ_{xx} denotes the resistivity along strike while ρ_{yy} denotes the resistivity across strike.

inverting MT data impacted by anisotropic structures, the location of individual conductors can be non-unique, even when using an anisotropic inversion. 2-D inversions of both southern profiles show evidence for a low resistivity layer in the upper mantle at depths of approximately 100 km.

11 INTERPRETATION OF RESISTIVITY MODELS AND DISCUSSION

11.1 Resistivity structure of the GSLsz

In the models presented above, the GSLsz is characterized by a high resistivity zone on all three profiles (Fig. 14), sometimes flanked by conductors. The width of this zone is 20–40 km, somewhat larger than the interstation spacing. Thus the actual width of the resistor could be narrower but it cannot be resolved with the current data set. A number of factors can cause high or low resistivity in a fault zone. Fault zone deformation close to the surface can produce elevated porosities, and result in a low resistivity if the cracks are filled with aqueous fluids (e.g. the damaged zone in the upper 2 km of the SAF). At greater depth there is evidence that mylonites can exhibit elevated porosity when exhumed from mid-crustal depths (Wibberley & Shimamoto 2003). However many rocks formed at depth under high pressure and temperature, such as the mylonites in the GSLsz, exhibit very low porosity. This low porosity, combined with the loss of aqueous fluids during deformation and annealing could result in a high resistivity (Altenberger & Kruhl 2000). However, many shear zones contain abundant graphite films deposited

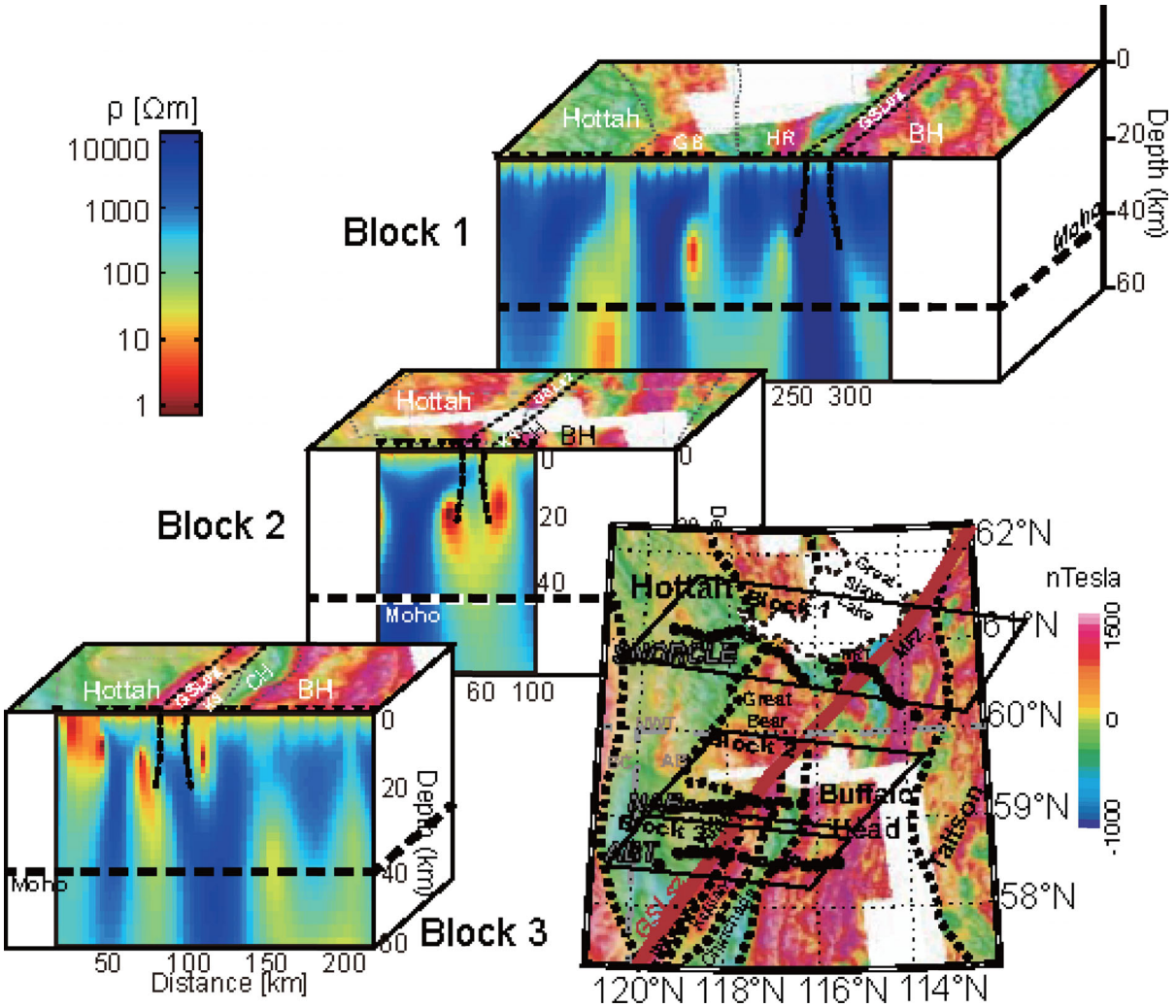

Figure 14. A 3-D schematic of variations in resistivity structure along the GSLsz. The surface of each block shows the co-incident aeromagnetic anomaly (modified from Ross & Eaton 2001).

on grain boundaries, resulting in a very low, often anisotropic, resistivity structure. Thus if the resistive zone in the GSLsz is associated with mylonites formed at depth within the shear zone, then the graphite must have somehow been removed, or deposited in non-connected films. Recent laboratory studies by Yoshino & Noritake (2011) showed that graphite films will cease to be interconnected above 700 °C. This corresponds to granulite facies which form a significant proportion of the GSLsz mylonites. This explanation for the high resistivity would require that no reconnection of graphite films occurred during subsequent cooling and exhumation. A non-continuous distribution of graphite from greenschists within the GSLsz has been observed (Simon Hanmer, personal communication, 2014). If electric current is transported by surface effects, then it is possible that grain size may control the resistivity (ten Grotenhuis *et al.* 2004). In the context of a shear zone, mylonites would be fine grained (Warren & Hirth 2006) and could make a significant reduction to the resistivity under low porosity conditions.

In summary, the high resistivity of the mylonites suggests that grain boundary effects do not contribute to the resistivity, and that interconnected graphite films are not present in the rocks found in the core of the GSLsz. There is some evidence that the resistive core is flanked by conductors that may be zones of localized deformation. However, the station spacing is insufficient to resolve these details.

The 2-D resistivity model of the SNORCLE profile is superposed on the model of Sibson (1977; Fig. 15) and may help to understand the geometry of the GSLsz since the its upper crustal part had been eroded.

11.2 Low resistivity/electrical anisotropy beneath the GSLsz

The inversion models derived from the MT profiles in Alberta (ABT and NAB) are quite distinct from the model for the SNORCLE profile, and exhibit a low resistivity layer, likely anisotropic, that extends beneath the GSLsz (Fig. 16). The 2-D inversions image this layer as a set of discrete conductors that form an east dipping anisotropic layer. The anisotropy of the layer has the low resistivity parallel to strike. It appears that the GSLsz may cut the dipping anisotropic layer, implying that it is younger.

11.3 Explanations for along-strike variations in electrical structure

The along-strike variations in crustal resistivity structure of the GSLsz revealed by this study may be caused by a range of tectonic

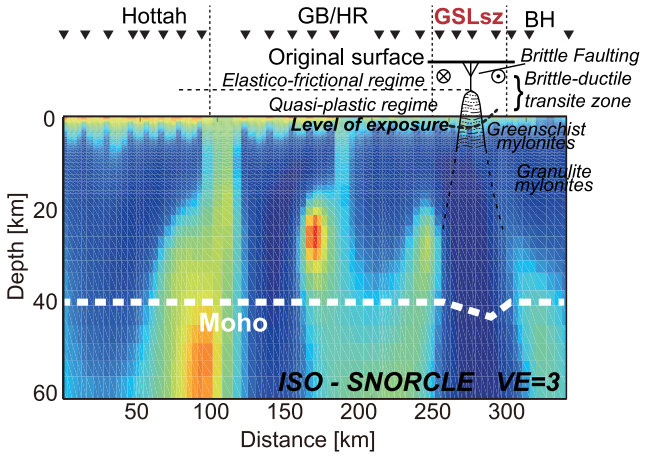

Figure 15. Interpretation of the electrical resistivity structure on the SNORCLE profile, based on the 2-D inversion model. Vertical exaggeration is 3:1. The resistivity model is superposed on inferred shear zone structure based on Sibson (1977) and Hanmer (1988).

processes in different parts of the shear zone. Combined with other geological and geophysical information, three possible explanations for the along-strike variations in electrical structure are discussed as follows.

11.3.1 Different structural levels exposed in different locations

Sibson (1977) proposed that shear zones broaden with depth and deformation changes from narrow brittle faults to distributed plastic deformation. The depth at which the shear zone changes character may even place constraints on the depth of the brittle–plastic transition. Hanmer (1988) showed that the exposed central segment of the GSLsz was characterized by broad zones of high grade mylonites, dissected by narrow zones of younger, lower grade mylonites that formed at shallower depths. This gave strong evidence that the GSLsz had been syntectonically exhumed as it developed. Is it possible that the amount of exhumation has varied along strike? The exhumation of metamorphic rocks beneath a shear zone has previously been considered to generate large amounts of fluids as well as those generated during heating processes associated with burial of rocks (Vry *et al.* 2010). High electrical conductivity anomalies observed in the Southern Alps in New Zealand were interpreted as fluids (Davey *et al.* 1998; Wannamaker *et al.* 2002). After shearing deformation and exhumation the fluids probably would have vanished from the shear zone by erosion. There still could be conductive materials (e.g. graphite) left behind, which can lower the present-day resistivity. However, the spatial distribution of the conductive/anisotropic layer is unlikely to be due to the processes associated with the burial or exhumation of the shear zone. This is because the dipping low resistivity layer is more than 100 km wide and much broader than the 25 km width of GSLsz determined from outcrop (Hanmer 1988). Thus, a differential exhumation level cannot readily explain the different resistivity structure observed on the GSLsz in the NWT and NW Alberta.

11.3.2 Different tectonic processes occurred in different locations

The GSLsz separates a region of accretionary tectonics to the south and indentation—escape tectonics to the north (Ross & Eaton 2002; Fig. 2b). The lack of a dipping anisotropic layer beneath the SNORCLE MT line is supported by the absence of a feature in teleseismic data collected some 100 km to the northeast (Snyder & Kjarsgaard 2013), although a small feature may not be imaged by the teleseismic data. As mentioned above, a broad zone of mylonites characterizes the central segment, and this requires an extensive period of shear deformation.

In contrast, the tectonic history recorded in the basement rocks of NW Alberta began with convergence in the Proterozoic as crustal elements were joined together by accretionary tectonics (Ross 1990). The Ksituin and Kiskatinaw terranes were added to the BHT around 1.987–1.900 Ga (Ross 1990; Ross & Eaton 2002). Further south, this accretion process was studied as part of the PRAISE reflection survey (Ross & Eaton 1997; Hope *et al.* 1999) and the pattern of dipping zones with high reflectivity were inferred to be due to the imbrication of a number of crustal terranes (Ross 1990, 2002). Subduction could have also formed the east dipping, low resistivity layer observed in the MT data beneath the NAB and ABT profiles, as crustal material was underthrust beneath the Rae craton (BHT). In this scenario, the electrical anisotropy would have resulted from preferred orientations of fracture porosity or graphitized shear zones on the thrust contact. This phenomenon has been invoked in other studies as an explanation of electrical anisotropy in thrust zones (Jones 1992; Kellett *et al.* 1992; Kurtz *et al.* 1993; Mareschal *et al.* 1994, 1995; Boerner *et al.* 2000a,b). Boerner *et al.* (1999) interpreted the conducting material to be graphite precipitated from mantle CO_2 fluxes along crustal scale fault zones, while a predominantly biogenic component was suggested by Mareschal *et al.* (1994). Graphitic films along shear zones and hydrous defects in olivine were offered as possible mechanisms for the electrical anisotropy of the GSLsz (Eaton *et al.* 2004; Wannamaker 2005). In the North American Central Plains (NACP) within the Proterozoic Trans Hudson orogen (Camfield & Gough 1977; Wu *et al.* 1993; Jones *et al.* 1993, 1997, 2005), electrical anisotropy observed in central Saskatchewan was interpreted as sulphide minerals remobilized into fold hinges. Another mechanism that could cause the subducted plate to be anisotropic could be the seawater filled cracks formed as the plate bent in the subduction zone (Key *et al.* 2012). While the seawater would be rapidly expelled with pressure during subduction, this could provide a fabric for the deposition of a conducting phase that could cause electrical anisotropy.

In summary, support for the hypothesis that the GSLsz in northwestern Alberta is underlain by a major east dipping thrust comes from the fact that the low resistivity anomaly dips east, is anisotropic and extends well outside the surface extent of the GSLsz.

11.3.3 Subsequent modification or fault zone reactivation

There is evidence that the GSLsz underwent reactivation during the Phanerozoic. Far- field stress related to the Devonian–Carboniferous Antler and Late Cretaceous–Palaeogene Laramide orogenies may have formed or reactivated the HRfz within the wide corridor of Proterozoic crustal weakness (GSLsz). This has influenced the deposition of the overlying sedimentary rocks (Hathway *et al.* 2013) and possibly led to the formation of oil and gas traps adjacent to the HRfz (Peirce *et al.* 2001). Reef development and the flow of hot fluids causing hydrothermal dolomitization may have also been controlled by this reactivation e.g. in the Rainbow Basin as described by Peirce *et al.* (2001). The dolomitization and metallic mineral deposition of the Pine Point ore body, near the GSLsz on the SNORCLE corridor, would have required large volumes of mineralizing fluids (Peirce *et al.* 2001). Basinal and meteoric fluids would have moved though both the sedimentary rocks of the WCSB and the underlying basement rocks in zones with elevated permeability, including

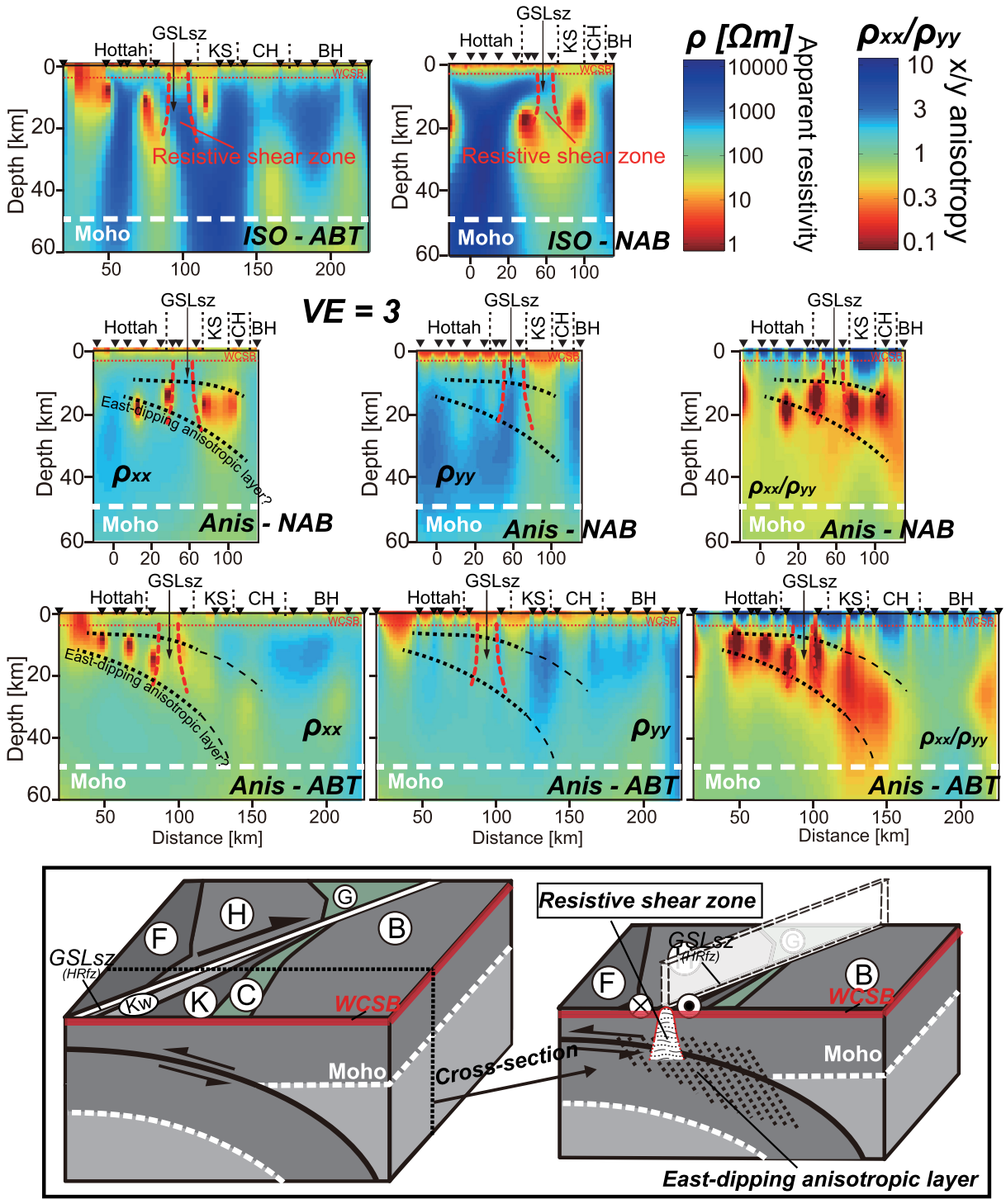

Figure 16. The interpretation of the electrical structure of the GSLsz across NAB and ABT profiles. Vertical exaggeration is 3:1.

fault zone rocks (Pană 2006). Such fluids could cause low resistivity in the shallow structural level of fault/shear zones, if still water saturated, or if the fluids deposited conducting phases. One of the most probable processes which can enhance the permeability of the basement rocks is shearing, particularly at dilational jogs of strike-slip faults. However, the low resistivity areas shown in the inversion models are much broader than the shear zone, and the permeability of the basement rocks outside the shear zone area is likely too low to reduce the resistivity if originally undeformed (Brace 1980).

12 DISCUSSION

Taking all of the geological and geophysical information into account, hypothesis (ii) is the preferred model to explain the resistivity structure of the GSLsz in northwestern Alberta (Fig. 16). The east-dipping anisotropic conductors were formed by eastward subduction during Palaeoproterozoic terrane accretion and thrusting. The BHT and Chinchaga domain were accreted between 1.999 and 1.993 Ga (Ross 1990), followed by the collision between the

Ksituan domain and the Buffalo Head- Chinchaga composite domain at 1.972–1.900 Ga (Eaton *et al.* 1999). Some authors have proposed that the Slave Craton was also involved in this phase of convergence (Hanmer *et al.* 1995). The elevated conductivity of the dipping layer is likely caused by sulphide minerals and/or graphite preferentially deposited on folds within the thrusts, as proposed to explain the major conductor found within the Trans-Hudson Orogen (Jones *et al.* 1997).

At some later time, strike-slip motion on the GSLsz would have disturbed the east dipping anisotropic conductors. The early ductile phase of deformation on the GSLsz occurred at 1.990–1.920 Ga on the NE segment (Hoffman 1987) and overlaps in time with the accretion events listed above. However, the phase of brittle deformation on the GSLsz occurred significantly later at 1.840–1.750 Ga, and could have disrupted the east-dipping conductive anisotropic structures. Once the upper crust was removed by erosion, the granulite facies rock formed in the lower crust would have been exposed at the surface. Initial deformation of the granitoid protolith under granulite facies conditions would have expelled most of the volatiles ($H_2O + CO_2$) leaving a resistive granulite mylonite. As the initial granulite raised through the crust during *ca*. 70 Myr of syntectonic exhumation, new granulite facies mylonite was continually formed in the deep structural levels of the evolving GSLsz. The distribution of mylonite belts at the surface (Hanmer 1988; Hanmer *et al.* 1992) suggests a subvertical wall of anhydrous granulite facies rocks possibly crosscut by retrogressive amphibolite facies mylonite belts at mid-crustal levels and narrower greenschist facies mylonite belts in the upper crust. The propagation of this volatile-depleted high strain zone into the upper mantle could explain the resistivity model that shows a resistive shear zone cutting through the conductive/anisotropic layer on the NAB and ABT profiles. In this model, the lack of dipping anisotropic conductors on the central GSLsz (SNORCLE profile) can be explained by tectonics dominated by pure strike-slip motion, with no convergence. Some vertical motion might have occurred at this stage, but the broad inter station spacing and long periods used in the field do not allow such a feature to be detected.

This transition of a convergent margin into a transform margin can be seen elsewhere in the geologic record. The Sumatra–Andaman Plate boundary is a modern analog for the subduction and subsequent strike-slip faulting history in northwest Alberta. In this setting, the Australian plate subducts northward beneath Eurasia with the strike-slip component of motion offset accommodated on the trench parallel Sumatra fault (McCaffrey 2009). A later stage example can be found on the west coast of North America, where over the last 30 Ma a subduction zone has been transformed into a primarily strike-slip boundary that is characterized today by the San Andreas Fault (Atwater 1970). Seismic studies have shown that the San Andreas Fault likely extends to the depth of the former suducting slab (Howie *et al.* 1993). Thus the model of Sibson (1977) can only be applied to depths from the surface to that of the subducted plate.

13 CONCLUSIONS

The analysis of the MT data collected on three profiles crossing the GSLsz reveal along-strike variations in crustal resistivity structure. Isotropic and anisotropic 2-D inversions and isotropic 3-D inversions show markedly different resistivity structures on the segments of the shear zone in the Northwest Territories and northwestern Alberta. The GSLsz is imaged as a high resistivity zone (>5000 Ωm) on all three profiles. On the SNORCLE profile, it is at least 20 km wide to a depth of at least 50 km. The resistive zones of the ABT and NAB profiles appear to be confined to the crust and pierce an, east-dipping, crustal conductor at 20–25 km depth. Combined with the results of the dimensionality analysis, this conductor appears to be anisotropic, likely caused by conductive materials filling in the networks of fractures with preferred orientation within a former suduction zone at 1.97–190 Ga. These conductive regions would have then been disrupted by strike-slip, ductile deformation on the GSLsz that occurred at 1.9–1.75 Ga under high-grade metamorphic conditions (granulite facies). This can explain why the GSLsz appears as a resistive structure piercing the dipping anisotropic layer. The high resistivity rock is consistent with anhydrous mylonites, and it is possible that graphite is present, but not interconnected owing to the high temperatures experienced during deformation. The lack of accretion further north on the central GSLsz can be inferred from the absence of a similar anisotropic/conductive layer in this region, a hypothesis supported by recent teleseismic data.

ACKNOWLEDGEMENTS

This research was supported by an NSERC Discovery Grant awarded to Martyn Unsworth, and also by funding from Natural Resources Canada under the auspices of the GEM program and the Alberta Geological Survey, Alberta Energy Regulator. The 3-D MT inversions were made possible with the high-performance clusters operated by Compute Canada. Yaotian Yin acknowledges support from the China Scholarship Council. The development of some methods used in this research was supported by SinoProbe-01&02 projects funded by Chinese government. We thank Greg Nieuwenhuis, Monica Doorenboos and Daniel Gamble for help in the field. We thank Alan Jones and Gary NcNeice for use of their tensor decomposition software. Simon Hanmer, David Snyder, David Eaton and Rob Evans are thanked for their constructive reviews.

REFERENCES

Altenberger, U. & Kruhl, J.H., 2000. Dry high-temperature shearing in the fossil Hercynian lower crust of Calabria (southern Italy), *Per. Mineral.,* **69,** 125–142.

Armijo, R. *et al.*, 1999. Westward propagation of the North Anatolian fault into the northern Aegean: timing and kinematics, *Geology,* **27**(3), 267–270.

Atwater, T., 1970. Implications of plate tectonics for the Cenozoic tectonic evolution of Western North America, *GSA Bulletin,* **81,** 3513–3536.

Aulbach, A., Griffin, W.L. & O'Reilly, S.Y., 2003. Comparative Cratonology in Canada: slave against Buffalo, Research Highlights 2003 of ARC National Key Centre for Geochemical Evolution and Metallogeny of Continents (GEMOC), Macquarie University.

Aulbach, A., Griffin, W.L., O'Reilly, S.Y. & McCandless, T.E., 2004. Genesis and evolution of the lithospheric mantle beneath the Buffalo Head Terrane, Alberta (Canada), *Lithos,* **77,** 413–451.

Bai, D. *et al.*, 2010. Crustal deformation of the eastern Tibetan plateau revealed by magnetotelluric imaging, *Nat. Geosci.,* **3,** 358–362.

Becken, M., Ritter, O., Park, S.K., Bedrosian, P.A., Weckmann, U. & Weber, M., 2008. A deep crustal fluid channel into the San Andreas Fault system near Parkfield, California, *Geophys. J. Int.,* **173,** 718–732.

Bedrosian, P.A., Unsworth, M.J. & Wang, F., 2001. Structure of the Altyn Tagh Fault and Daxue Shan from magnetotelluric surveys: implications for faulting associated with the rise of the Tibetan Plateau, *Tectonics,* **20**(4), 474–486.

Bedrosian, P., Unsworth, M., Egbert, G. & Thurber, C., 2004. Geophysical images of the creeping segment of the San Andreas Fault: implications for the role of crustal fluids in the earthquake process, *Tectonophysics,* **385,** 137–158.

Berman, R.G., Pehrsson, S., Davis, W.J., Ryan, J.J., Qui, H. & Ashton, K.E., 2013. The Arrowsmith orogeny: geochronological and thermobarometric constraints on its extent and tectonic setting in the Rae craton, with implications for pre-Nuna supercontinent reconstruction, *Precambrian Res.,* **232,** 44–69.

Bertrand, E.A. *et al.*, 2012a. Magnetotelluric imaging beneath the Taiwan orogen: an arc-continent collision, *J. geophys. Res.,* **117,** B01402, doi:10.1029/2011JB008688.

Bertrand, E.A. *et al.*, 2012b. Magnetotelluric imaging of upper-crustal convection plumes beneath the Taupo Volcanic Zone, New Zealand, *Geophys. Res. Lett.,* **39,** L02304, doi:10.1029/2011GL050177.

Boerner, D.E., Kurtz, R.D., Craven, J.A., Ross, G.M., Jones, F.W. & Davis, W.J., 1999. Electrical conductivity in the Precambrian lithosphere of Western Canada, *Science,* **283,** 668–670.

Boerner, D.E., Kurtz, R.D. & Craven, J.A., 2000a, A summary of electromagnetic studies on the Abitibi-Grenville transect, *Can. J. Earth Sci.,* **37,** 427–437.

Boerner, D.E., Kurtz, R.D., Craven, J.A., Ross, G.M. & Jones, F.W., 2000b. A synthesis of electromagnetic studies in Lithoprobe Alberta Basement Transect: constraints on Paleoproterozoic indentation tectonics, *Can. J. Earth Sci.,* **37,** 1509–1534.

Bowring, S.A., Van Schmus, W.R. & Hoffman, P.F., 1984. U-Pb zircon ages from Athapuscow aulacogen, east arm of Great Slave Lake, *Can. J. Earth Sci.,* **21,** 1315–1324.

Brace, W.F., 1980. Permeability of crystalline and argillaceous rocks, *Int. J. Rock Mech. Min. Sci. Geomech. Abstr.,* **17**(5), 241–251.

Brasse, H. & Soyer, W., 2001. A magnetotelluric survey in the Southern Chilean Andes, *Geophys. Res. Lett.,* **28,** 3757–3760.

Caldwell, T.G., Bibby, H.M. & Brown, C., 2004. The magnetotelluric phase tensor, *Geophys. J. Int.,* **158,** 457–469.

Camfield, P.A. & Gough, D.I., 1977. A possible Proterozoic Plate boundary in North America, *Can. J. Earth Sci.,* **14,** 1229–1238.

Chacko, T., De, K.S., Creaser, R.A. & Muehlenbachs, K., 2000. Tectonic setting of the Taltson magmatic zone at 1.9–2.0 Ga: a granitoid-based perspective, *Can. J. Earth Sci.,* **37,** 1597–1609.

Davey, F. *et al.*, 1998. Preliminary results from a geophysical study across a modern continent–continent collisional plate boundary—the Southern Alps, New Zealand, *Tectonophysics,* **288,** 221–235.

De, K.S., Chacko, T., Creaser, R.A. & Muehlenbachs, K., 2000. Geochemical and Nd-Pb-O isotope systematics of granites from the Taltson magmatic zone, NE Alberta: implications for Early Proterozoic tectonics in western Laurentia, *Precambrian Res.,* **102,** 221–249.

Eaton, D.W. & Hope, J., 2003. Structure of the crust and upper mantle of the Great Slave Lake shear zone, northwestern Canada, from teleseismic analysis and gravity modeling, *Can. J. Earth Sci.,* **40,** 1203–1218.

Eaton, D.W., Ross, G.M. & Hope, J., 1999. The rise and fall of a Cratonic arch: a regional perspective on the Peace River Arch, Alberta, *Bull. Can. Petrol. Geol.,* **47,** 346–361.

Eaton, D.W., Jones, A.G. & Ferguson, I.J., 2004. Lithospheric anisotropy structure inferred from collocated teleseismic and magnetotelluric observations: Great Slave Lake shear zone, northern Canada, *Geophys. Res. Lett.* **31,** L19614, doi:10.1029/2004GL020939.

Eisel, M. & Bahr, K., 1993. Electrical anisotropy in the lower crust of British Columbia: an interpretation of a magnetotelluric profile after tensor decomposition, *J. Geomagn. Geoelectr.,* **45,** 1115–1126.

Eisel, M., Haak, V., Pek, J. & Cerv, V., 2001. A magnetotelluric profile across the German Deep Drilling Project (KTB) area: two- and three-dimensional modeling results, *J. geophys. Res.,* **106,** 16 061–16 073.

Egbert, G.D., 1997. Robust multiple-station magnetotelluric data processing, *Geophys. J. Int.,* **130**(2), 475–496.

Egbert, G.D. & Booker, J.R., 1986. Robust estimation of geomagnetic transfer functions, *Geophys. J. R. astr. Soc.,* **87,** 173–194.

Gabrielse, H., Murphy, D.C. & Mortensen, J.K., 2006. Cretaceous and Cenozoic dextral orogen-parallel displacements, magmatism, and paleogeography, north-central Canadian Cordillera, *Paleogeography of the North American Cordillera: Evidence For and Against Large-Scale Displacements: Geological Association of Canada, Special Paper,* **46,** 255–276.

Gamble, T.D., Goubeau, W.M. & Clarke, J., 1979. Magnetotellurics with a remote reference, *Geophysics,* **44,** 53–68.

Geiger, H.D. & Cook, F.A., 2001. Analysis of crustal structure from bandpass and directionally filtered potential field data: an example from western Canada, *Can. J. Earth Sci.,* **38,** 953–961.

Geological Survey of Canada. 1981. Magnetic Anomaly Map, Lockhart River, NWT, map NP 12–13 1566A, scale 1:1,000,000. Geological Survey of Canada.

Geological Survey of Canada. 1984. Magnetic Anomaly Map, Slave River, NWT, map NP 11–12-M, scale 1:1,000,000. Geological Survey of Canada.

Geological Survey of Canada. 1987. Magnetic Anomaly Map of Canada, map 1255A, scale 1:5,000,000. Geological Survey of Canada.

Gibb, R.A., 1978. Slave–Churchill collision tectonics, *Nature (London),* **271,** 50–52.

Groom, R.W. & Bailey, R.C., 1989. Some effects of multiple lateral inhomogeneities in magnetotellurics, *Geophys. Prospect.,* **37,** 697–712.

Hanmer, S., 1988. Great Slave Lake shear zone, Canadian Shield: reconstructed vertical profile of a crustal-scale fault zone, *Tectonophysics,* **149,** 245–264.

Hanmer, S. & Connelly, J.N., 1986. Mechanical role of the syntectonic Laloche Batholith in the Great Slave Lake shear zone, District of Mackenzie, NWT, in *Current Research. Geological Survey of Canada,* **Paper 86–1B**, pp. 21–26.

Hanmer, S. & Lucas, S.B., 1985. Anatomy of a ductile transcurrent shear: the Great Slave Lake shear zone, District of Mackenzie, NWT, in *Current Research. Geological Survey of Canada,* **Paper 85–1B**, pp. 7–22.

Hanmer, S. & Needham, T., 1988. Great Slave Lake shear zone meets Thelon Tectonic Zone, District of Mackenzie, NWT, in *Current Research. Geological Survey of Canada,* **88**(1c), 33–49.

Hanmer, S., Bowring, S., van Breemen, O. & Parrish, R., 1992. Great Slave Lake shear zone, NW Canada: mylonitic record of Early Proterozoic continental convergence, collision and indentation, *J. Struct. Geol.,* **14,** 757–774.

Hanmer, S., Williams, M. & Kopf, S., 1995. Striding-Athabasca mylonite zone: implications for the Archean and Early Proterozoic tectonics of the Western Canadian Shield, *Can. J. Earth Sci.,* **32,** 178–196.

Harris, J.B., 2009. Hammer-impact SH-wave seismic reflection methods in neotectonic investigations: general observations and case histories from the Mississippi Embayment, U.S.A., *J. Earth Sci.,* **20,** 513–525.

Hathway, B., Dolby, G., McNeil, D.H., Kamo, S.L., Heizler, M.T. & Joyce, N., 2013. Revised stratigraphy, regional correlations and new bentonite radiometric ages for the Albian Loon River Formation, Fort St. John Group, northwestern Alberta, *Bull. Can. Petrol. Geol.,* **61**(4), 331–358.

Heise, V. & Pous, J., 2001. Effects of anisotropy on the two-dimensional inversion procedure, *Geophys. J. Int.,* **147,** 610–621.

Heise, W., Caldwell, T.G., Bibby, H.M. & Brown, C., 2006. Anisotropy and phase splits in magnetotellurics, *Phys. Earth planet. Inter.,* **158**(2–4), 107–121.

Hickman, S., Zoback, M. & Ellsworth, E., 2004. Introduction to special section: preparing for the San Andreas Fault Observatory at Depth, *Geophys. Res. Lett.,* **31,** L12S01, doi:10.1029/2004GL020688.

Hoffman, P.F., 1980. A Wilson cycle of early Proterozoic age in the northwest of the Canadian Shield, in *The Continental Crust and its Mineral Deposits: Geological Association of Canada Special Paper* **20,** pp. 523–549.

Hoffman, P.F., 1987. Continental transform tectonics: Great Slave Lake shear zone (ca. 1.9 Ga), northwest Canada, *Geology,* **15,** 785–788.

Hoffman, P.F., 1988. United plates of America, the birth of a craton: early Proterozoic assembly and growth of Proto-Laurentia, *Ann. Rev. Earth planet. Sci.,* **16,** 543–603.

Hoffman, P.F., 1989. Precambrian geology and tectonic history of North America, in *The Geology of North America—An Overview,* Vol. A, pp. 447–512, eds Bally, A.W. & Palmer, A.R., Geological Society of America.

Hoffman, P.F., Bell, I.R., Hildebrand, R.S. & Thorstad, L, 1977. Geology of Athapuscow Aulacogen, East Arm of Great Slave Lake, District of Mackenzie, in *Current Research, Part A, Geological Survey of Canada,* **Paper 77–1A**, pp. 117–129.

Hoffman, P.F. *et al.*, 1986. Is the Thelon Front (NWT) a suture? *GAC-MAC Joint AMU. Meet., Progr. Abstr.,* p. 82.

Hoffman-Rothe, A., Ritter, O. & Janssen, C., 2004. Correlation of electrical conductivity an structural damage at a major strike-slip fault in Northern Chile, *J. geophys. Res.,* **109**, doi:10.1029/2004JB003030.

Hope, J. & Eaton, D., 2002. Crustal structure beneath the Western Canada Sedimentary Basin: constraints from gravity and magnetic modelling, *Can. J. Earth Sci.,* **39,** 291–312.

Hope, J., Eaton, D.W. & Ross, G.M. 1999. Lithoprobe seismic transect of the Alberta Basin: compilation and interregional analysis, *Bull. Can. Petrol. Geol.,* **47,** 331–345.

Howie, J.M., Miller, K.C. & Savage, W.U., 1993. Integrated crustal structure across the south central California margin: Santa Lucia Escarpment to the San Andreas fault, *J. geophys. Res.,* **98,** 8173–8196.

Janssen, C., Hoffmann-Rothe, A., Tauber, S. & Wilke, H., 2002. Internal structure of the Precordilleran fault system (Chile)—insights from structural and geophysical observations, *J. Struct. Geol.,* **24,** 123–143.

Jones, A.G., 1992. Electrical properties of the continental lower crust, in *Continental Lower Crust,* pp. 81–143, eds Fountain, D.M., Arculus, R.J. & Kay, R.W., Elsevier.

Jones, A.G., 2006. Electromagnetic interrogation of the anisotropic Earth: looking into the Earth with polarized spectacles, *Phys. Earth planet. Inter.,* **158**(2–4), 281–291.

Jones, A.G. & Craven, J.A., 2004. Area selection for diamond exploration using deep-probing electromagnetic surveying, *Lithos,* **77,** 765–782.

Jones, A.G. & Gough, D.I., 1995. Electromagnetic images of crustal structures in southern and central Canadian Cordillera, *Can. J. Earth Sci.,* **32**(10), 1541–1563.

Jones, A.G., Craven, J.A., McNiece, G.W., Ferguson, I.J., Boyce, T., Farquarson, C. & Ellis, R., 1993. North American Central Plains conductivity anomaly within the trans-Hudson Orogen in Northern Saskatchewan, Canada, *Geology,* **21,** 1027–1030.

Jones, A.G., Katsube, T.J. & Schwann, P., 1997. The longest conductivity anomaly in the world explained: sulphides in fold hinges causing very high electrical anisotropy, *J. Geomagn. Geoelectr.,* **49,** 1619–1629.

Jones, A.G., Ferguson, I.J., Chave, A., Evans, R. & Mcneice, G., 2001. Electrical lithosphere of the Slave craton, *Geology,* **29,** 423–426.

Jones, A.G., Lezaeta, P., Ferguson, I.J., Chave, A.D., Evans, R.L., Garcia, X. & Spratt, J. 2003. The electrical structure of the Slave craton, *Lithos,* **71,** 505–527.

Jones, A.G., Ledo, J. & Ferguson, I.J., 2005. Electromagnetic images of the Trans-Hudson orogen: the North American Central Plains anomaly revealed, *Can. J. Earth Sci.,* **42,** 457–478.

Kellett, R.L., Mareschal, M. & Kurtz, R.D., 1992. A model of lower crustal electrical anisotropy for the Pontiac Subprovince of the Canadian Shield, *Geophys. J. Int.,* **111,** 141–150.

Key, K., Constable, S., Matsuno, T., Evans, R.L. & Myer, D., 2012. Electromagnetic detection of plate hydration due to bending faults at the Middle America Trench, *Earth planet. Sci. Lett.,* **351–352,** 45–53.

Kirkwood, S.E., Hutton, V.R.S. & Sik, J., 1981. A geomagnetic study of the Great Glen fault, *Geophys. J.R. astr. Soc.* **66,** 481–490.

Kurtz, R.D., Craven, J.A., Niblett, E.R. & Stevens, R.A., 1993. The conductivity of the crust and mantle beneath the Kapuskasing Uplift: electrical anisotropy in the upper mantle, *Geophys. J. Int.,* **113,** 483–498.

Mackie, R.L., Smith, J.T. & Madden, T.R., 1994. Three-dimensional electromagnetic modeling using finite difference equations: the magnetotelluric example, *Radio Sci.,* **29,** 923–935.

Majorowicz, J.A., Gough, D.I. & Lewis, T.J., 1993. Correlation between the depth to the lower-crustal high conductive layer and heat flow in the Canadian Cordillera, *Tectonophysics,* **225,** 49–56.

Mareschal, M., Kurtz, R.D. & Bailey, R.C., 1994. A review of electromagnetic investigations in the Kapuskasing uplift and surrounding regions: electrical properties of key rocks, *Can. J. Earth Sci.,* **31,** 1042–1051.

Mareschal, M., Kellett, R., Kurtz, R.D., Ludden, J.N., Ji, S. & Bailey, R.C., 1995. Archean cratonic roots, mantle shear zones and deep electrical anisotropy, *Nature,* **375,** 134–137.

McCaffrey, R., 2009. The Tectonic framework of the Sumatran subduction zone, *Annu. Rev. Earth planet. Sci.,* **37,** 345–366.

McNeice, G. & Jones, A.G., 2001. Multisite, multifrequency tensor decomposition of magnetotelluric data, *Geophysics,* **66,** 158–173.

McBride, J.H. & Brown, L.D., 1986. Reanalysis of the cocorp deep seismic reflection profile across the SAF, Parkfield, California, *Bull. seism. Soc. Am.,* **76,** 1668–1686.

Meqbel, N.M.M. & Ritter, O. DESIRE Group, 2013. A magnetotelluric transect across the Dead Sea Basin: electrical properties of geological and hydrological units of the upper crust, *Geophys. J. Int.,* **193**(3), 1415–1431.

Muir, I.D. & Dravis, J.J., 1992. Burial porosity development in middle Devonian Keg River reservoirs, Lithoprobe Alberta Basement Transects Workshop, Report 28, pp. 102–103.

Pană, D., 2006. Unravelling the structural control of Mississippi Valley-type deposits and prospects in carbonate sequences of the Western Canada Sedimentary Basin, *Geol. Surv. Can. Bull.,* **591,** 255–304.

Pană, D., Creaser, R.A., Muehlenbachs, K. & Wheatley, K., 2007. Basement geology in the Alberta portion of the Athabasca Basin, context for the Maybelle River area, in *EXTECH IV: Geology and Uranium Exploration Technology of the Proterozoic Athabasca Basin, Saskatchewan and Alberta, Geological Survey of Canada, Bulletin 588,* pp. 135–153.

Parkinson, W.D., 1962. The influence of continents and oceans on geomagnetic variations, *Geophys. J.R. astr. Soc.,* **6,** 411–449.

Pek, J. & Verner, T., 1997. Finite difference modelling of magnetotelluric fields in 2-D anisotropic media, *Geophys. J. Int.,* **128,** 505–521.

Peirce, J.W, Cordsen, A. & Glenn, T., 2001. The Great Slave Lake Shear Zone—implications for Exploration in NW Alberta and NE British Columbia, in *Canadian Society of Exploration Geophysicists Convention,* 2011.

Pilkington, M., Miles, W.F., Ross, G.M. & Roest, W.R., 2000. Potential-field signatures of buried Precambrian basement in the Western Canada sedimentary basin, *Can. J. Earth Sci.,* **37,** 1453–1471.

Plint, H.E. & Ross, G.M., 1993. $^{40}Ar/^{39}Ar$ geochronology of selected crystalline basement samples from the Alberta Basin: the timing of Proterozoic assembly of the subsurface of Western Canada: in Radiogenic age and isotopic studies, Report 7, *Geol. Surv. Canada,* **93**(2), 71–82.

Reinhardt, E.W., 1969. Geology of the Precambrian rocks of Tbubun Lakes map area in relationship to the McDonald fault system, district of Mackenzie (75E/12 and parts of 75E/13 and 85H/9), *Geol. Surv. Canada,* **29,** 69–21.

Rippe, D., Unsworth, M.J. & Currie, C.A., 2013. Magnetotelluric constraints on the fluid content in the upper mantle beneath the southern Canadian Cordillera: implications for rheology, *J. geophys. Res.: Solid Earth,* **118,** 5601–5624.

Ritter, O., Ryberg, T., Weckmann, U., Hoffmannrothe, A., Abueladas, A. & Garfunkel, Z. Desert Research Group, 2003a. Geophysical images of the Dead Sea transform in Jordan reveal an impermeable barrier for the fluid flow, *Geophys. Res. Lett.,* **30,** 1741, doi:10.1029/2003GL017541.

Ritter, O., Weckmann, U., Vietor, T. & Haak, V., 2003b. A magnetotelluric study of the Damara Belt in Namibia 1, regional scale conductivity anomalies, *Phys. Earth planet. Inter.,* **138,** 71–90.

Ritter, O., Hoffman-Rothe, A., Bedrosian, P.A., Weckmann, U. & Haak, V., 2004. Electrical conductivity images of active and fossil fault zones, in *Microstuctural Evolution and Physical Properties in High Strain Zones,* pp. 165–186, Geological Society of London Special Publications 245.

Rodi, W. & Mackie, R.L., 2001. Nonlinear conjugate gradients algorithm for 2D magnetotelluric inversion, *Geophysics,* **66,** 174–187.

Ross, G.M., 1990. Deep crust and basement structure of the Peace River Arch region: constraints on mechanisms of formation, *Bull. Can. Petrol. Geol.,* **38A,** 25–35.

Ross, G.M., 2002. Evolution of continental lithosphere in western Canada: a synthesis of lithoprobe studies in Alberta and beyond, *Can. J. Earth Sci.,* **39,** 413–437.

Ross, G.M. & Eaton, R.J., 1997. Winagami reflection sequence: seismic evidence for postcollisional migmatism in the Proterozoic of western Canada, *Geology,* **25-3,** 199–202.

Ross, G.M. & Eaton, D.W., 1999. Basement reactivation in the Alberta Basin: observational constraints and mechanical rationale, *Bull. Can. Petrol. Geol.,* **47,** 391–411.

Ross, G.M. & Eaton, D.W., 2001. Reply to comment: basement reactivation in the Alberta Basin, *Bull. Can. Petrol. Geol.,* **49,** 429–433.

Ross, G.M. & Eaton, D.W., 2002. Proterozoic tectonic accretion and growth of western Laurentia: results from Lithoprobe studies in northern Alberta, *Can. J. Earth Sci.,* **39,** 313–329.

Ross, G.M., Parrish, R.R., Villeneuve, M.E. & Bowring, S.A., 1991. Geophysics and geochronology of the crystalline basement of the Alberta Basement, western Canada, *Can. J. Earth Sci.,* **28,** 512–522.

Ross, G.M., Broome, J. & Miles, W., 1994. Potential fields and basement structure: Western Canada sedimentary basin, in *Geological Atlas of the Western Canada Sedimentary Basin. Calgary, Alta.: Can. Soc. Petr. Geol. and Alta. Res. Council,* pp. 41–46.

Ross, G.M., Eaton, D.W., Boerner, D.E. & Miles, W., 2000. Tectonic entrapment and its role in the evolution of the continental lithosphere: an example from the Precambrian of western Canada, *Tectonics,* **19,** 116–134.

Rutter, E., Brodie, K. & Evans, P., 1995. Structural geometry, lower crustal magmatic underplating and lithospheric stretching in the Ivrea-Verbano zone, northern Italy, *J. Struct. Geol.,* **15,** 647–662.

Sibson, R.H., 1977. Fault rocks and fault mechanisms, *J. Geol. Soc., Lond.,* **133,** 191–214.

Sibson, R.H., 1983. Continental fault structure and the shallow earthquake source, *J. Geol. Soc., Lond.,* **140,** 741–767.

Siripunvaraporn, W., Egbert, G., Lenbury, Y. & Uyeshima, M., 2005. Three-dimensional Magnetotelluric inversion: data-space method, *Phys. Earth planet. Inter.,* **150,** 3–14.

Soyer, W. & Unsworth, M.J., 2006. Deep electrical structure of the northern Cascadia (British Columbia, Canada) subduction zone: implications for the distribution of fluids, *Geology,* **34,** 53–56.

Snyder, D.B & Kjarsgaard, B.A., 2013. Mantle roots of major Precambrian shear zones inferred from structure of the Great Slave Lake shear zone, northwest Canada, *Lithosphere,* **5,** 539–546.

ten Grotenhuis, S.M., Drury, M.R., Peach, C.J. & Spiers, C.J., 2004. Electrical properties of fine-grained olivine: evidence for grain boundary transport, *J. geophys. Res.,* **109,** B06203, doi:10.1029/2003JB002799.

Tietze, K. & Ritter, O., 2013. Three-dimensional magnetotelluric inversion in practice—the electrical conductivity structure of the San Andreas Fault in Central California, *Geophys. J. Int.,* **195**(1), 130–147.

Türkoğlu, E., Unsworth, M.J. & Pana, D., 2009. Deep electrical structure of northern Alberta (Canada): implications for diamond exploration, *Can. J. Earth Sci.,* **46,** 139–154.

Unsworth, M. & Bedrosian, P.A., 2004a. Electrical resistivity structure at the SAFOD site from magnetotelluric exploration, *Geophys. Res. Lett.,* **31**, doi:10.1029/2003GL019405.

Unsworth, M. & Bedrosian, P.A., 2004b. On the geoelectric structure of major strike-slip faults and shear zones, *Earth Planets Space,* **56,** 1177–1184.

Unsworth, M.J., Egbert, G.D. & Booker, J.R., 1999. High Resolution electromagnetic imaging of the San Andreas Fault in Central California, *J. geophys. Res.,* **104,** 1131–1150.

Unsworth, M.J., Bedrosian, P., Eisel, M., Egbert, G.D. & Siripunvaraporn, W., 2000. Along strike variations in the electrical structure of the San Andreas fault at Parkfield, California, *Geophys. Res. Lett.,* **27,** 3021–3024.

Van Breemen, O., Thompson, P.H., Bostock, H.H. & Loveridge, W.D., 1987. Timing of plutonism in the northern Thelon tectonic zone and Taltson magmatic arc, *Geol. Assoc. Can. Prog. Abstracts,* **12,** 98.

Villeneuve, M.E., Ross, G.M., Thériault, R.J., Miles, W., Parrish, R.R. & Broome, J. 1993. Geophysical subdivision and U-Pb geochronology of the crystalline basement of the Alberta Basin, Western Canada, Geological Survey of Canada, Bulletin 447.

Vry, J., Powell, R., Golden, K.M. & Petersen, K., 2010. The role of exhumation in metamorphic dehydration and fluid production, *Nat. Geosci.,* **3**(1), 31–35.

Wannamaker, P.E., 2000. Comment on The petrologic case for a dry lower crust by Bruce, W.D. Yardley and John, W. Valley, *J. geophys. Res.,* **105,** 6057–6064.

Wannamaker, P.E., 2005. Anisotropy versus heterogeneity in Continental solid Earth electromagnetic studies: fundamental response characteristics and implications for physicochemical state, *Surv. Geophys.,* **26,** 733–765.

Wannamaker, P.E., Jiracek, G.R., Stodt, J.A., Caldwell, T.G., Gonzalez, V.M., McKnight, J.D. & Porter, A.D., 2002. Fluid generation and pathways beneath an active compression orogen, the New Zealand Southern Alps, inferred from magnetotelluric data, *J. Geophys. Res.,* **107**(B6), 2117, doi:10.1029/2001JB000186.

Warren, G.M. & Hirth, J., 2006. Grain size sensitive deformation mechanisms in naturally deformed peridotites, *Earth planet. Sci. Lett.,* **248,** 438–450.

Weckmann, U., Ritter, O. & Haak, V., 2003. A magnetotelluric study of the Damara Belt in Namibia 2. Internal structure of the Waterberg Fault/Omaruru Lineament, *Phys. Earth planet. Inter.,* **138,** 91–112.

Wibberley, C. & Shimamoto, T., 2003. Internal structure and permeability of major strike-slip fault zones: the Median Tectonic Line in Mie Prefecture, Southwest Japan, *J. Struct. Geol.,* **25,** 59–78.

Williams, R.A., Wood, S., Stephenson, W.J., Odum, J.K., Meremonte, M.E., Street, R. & Worley, D.M., 2003. Surface seismic-refraction/reflection measurements of potential site resonances and the areal uniformity of NEHRP site class D in Memphis, Tennessee, *Earthq. Spectra,* **19,** 159–189.

Wu, N., Booker, J.R. & Smith, J.T., 1993. Rapid two-dimensional inversion of COPROD2 data, *J. Geomag. Geoelectr.,* **45,** 1073–1087.

Wu, X., Ferguson, I.J. & Jones, A.G., 2002. Magnetotelluric response and geo-electric structure of the Great Slave Lake shear zone along SNORCLE corridor 1A, *Earth planet. Sci. Lett.,* **196,** 35–50.

Yardley, B.W.D. & Valley, J.W., 1997. The petrologic case for a dry lower crust, *J. geophys. Res.,* **102,** 12 173–12 185.

Yoshino, T. & Noritake, F., 2011. Unstable graphite films on grain boundaries in crustal rocks, *Earth planet. Sci. Lett.,* **306,** 186–192.